https://doi.org/10.5194/egusphere-2023-2156
Preprint. Discussion started: 25 September 2023

Holocene environmental and climate evolution of Central West Patagonia as reconstructed from lacustrine sediments of Meseta Chile Chico (46.5º S, Chile)

Carolina Franco[1], Antonio Maldonado[2], Christian Ohlendorf[1], A. Catalina Gebhardt[3], María Eugenia de Porras[4], Amalia Nuevo-Delaunay[5], César Méndez[5], Bernd Zolitschka[1]

[1] University of Bremen, Institute of Geography, GEOPOLAR, Bremen, Germany
[2] Centro de Estudios Avanzados en Zonas Áridas (CEAZA), La Serena, Chile
[3] Alfred Wegener Institute Helmholtz Centre for Polar and Marine Research, Bremerhaven, Germany
[4] IANIGLA, National Council of Scientific and Technical Investigations (CONICET), Mendoza, Argentina
[5] Centro de Investigación en Ecosistemas de la Patagonia (CIEP), Coyhaique, Chile

Correspondence to: Carolina Franco (cafranco@uni-bremen.de)

Abstract. Holocene environmental changes in Patagonia were mostly shaped by unsteady ice-cover recession. Consequently, environmental reconstructions are largely based on discontinuous moraine chronologies from valley deposits. Here, we present a 3 m-long continuous sediment record recovered from Laguna Meseta (LME), a lake located on Meseta Chile Chico. Its altitude and location relative to the North Patagonian Icefield provide a unique opportunity to reconstruct the glacial history and the related environmental dynamics.

Our radiocarbon chronology constrains sedimentation to the last ~10,000 years and provides a minimum age for postglacial ice-free lacustrine conditions due to a westward retreat of the ice cap. Lacustrine productivity reached its maximum at the start of sedimentation and decreased afterwards. Between 5,500 and 4,600 cal yr BP, a major shift towards allochthonous sediment accumulation occurred, caused by an abrupt increase in clastic deposition from basaltic lithologies of the Meseta Chile Chico. This episode correlates with the precipitation-driven mid-Holocene glacier advance of Patagonian glaciers and suggests that conditions were colder/wetter on the Meseta Chile Chico at that time. After 4,600 cal yr BP these conditions continued to supply LME with clastic sediments until a stepped decrease around 900 cal yr BP. Thereupon, lacustrine productivity distinctly increased and stabilized around 300 cal yr BP. Our findings indicate that environmental conditions on Meseta Chile Chico were mainly controlled by precipitation variability during regional oscillations of the Southern Hemisphere Westerly Winds over the last 10 ka.

Keywords: Lake sediments, Central West Patagonia, Middle Holocene, multiproxy analysis, precipitation, tephrochronology.

1 Introduction

The modern landscape of Patagonia is the result of climate-driven fluctuations of the large Patagonian Ice Sheet (Davies et al., 2020) that completely covered the Austral Andes during the Last Glacial Maximum (LGM) (Caldenius, 1932; Hulton et al., 1994; Rabassa et al., 2005). Throughout the Quaternary, glaciers of the Patagonian Ice Sheet advanced and retreated repetitively before splitting into the South and North Patagonian Icefields around 15 ka (Davies et al., 2020; Thorndycraft et al. 2019) as well as into several smaller ice caps distributed along the peaks of the Andean mountain range (Davies et al., 2020; Glasser et al., 2004; Sugden et al., 2005; Turner et al., 2005). However, after the end of accelerated ice recession mostly dated prior to the Pleistocene-Holocene transition (Bendle et al., 2017b; Davies et al., 2018; García et al., 2019), glacier fluctuations continued to occur.

https://doi.org/10.5194/egusphere-2023-2156
Preprint. Discussion started: 25 September 2023

Holocene climate variability resulted in regional glacier advances, still-stands or recessions, also referred to as "Neoglaciations" (Porter, 2000) that have been mostly studied based on moraine deposits in glacial valleys (Aniya, 1995; Clapperton and Sugden, 1988; Mercer, 1976). However, related chronologies are still subject of debate due to the discontinuity and asynchrony that entail moraine deposition and erosion as well as local topographic factors influencing glacier dynamics (Glasser et al., 2009).

Conversely, lacustrine sediments are continuous archives of environmental conditions. Therefore, we present a lacustrine sediment record from Meseta Chile Chico, a basaltic plateau covered by several small lakes. With a multiproxy sediment analysis, we aim to 1) constrain sedimentation dynamics of one of the lakes of this plateau throughout the Holocene; 2) use our results to reconstruct environmental history of the plateau and its surrounding area; 3) to establish correlations among environmental changes within our area, regional glacial oscillations, and paleoclimate proxies, with the objective of deriving insights into Holocene climatic variability in Central West Patagonia.

2 Regional Setting

2.1 Geology and Geomorphology

The Meseta Chile Chico is located in Central West Patagonia in the Región de Aysén, Chile (Fig. 1a), ca. 100 km east of the eastern margin of the North Patagonian Icefield (Fig. 1b). It is placed on the eastward slope of the easternmost mountain range of the Andes, the Parque Nacional Patagonia Range (Fig. 1c). The plateau, which lies between 1,100 and 2,000 m a.s.l., ranges from Cerro Pico Sur in the north and ends at the western slopes of the valley of Río Jeinemeni. Due to its altitude and morphology, the environment of Meseta Chile Chico is less influenced by local factors such as surrounding topography, vegetation and human intervention (Méndez et al., 2023) compared to the surrounding glacial valleys. Additionally, this plateau is covered with several small lakes (Fig. 2a), which are interconnected by meadows, ephemeral rivers and form part of its drainage basin that currently drains into Río Jeinemeni. Today it is mostly fed by snowmelt and rain. Nevertheless, several (today empty) glacial cirques that occur in the Meseta Chile Chico catchment as well as their topographic connections with the Cerro Las Nieves glaciers to the west indicate past glacial influence for this area (Fig. 1c).

Most of Meseta Chile Chico is formed by alkaline flood basalts of Miocene age, defined as the Upper Basalts of Meseta Chile Chico. Furthermore, at the northern border of Meseta Chile Chico, in the watershed of Arroyo Cardenio and in the Cerro las Nieves-Cerro Pico Sur range as well as at some of its eastern flanks, older Paleocene-Eocene basaltic rocks of the Lower Basalts of the Meseta Chile Chico crop out (Fig 2a). These rocks are (partly) covered by unconsolidated Holocene moraine deposits (Fig 1.c, Espinoza et al., 2005; De la Cruz y Suárez, 2008) distributed along the entire Meseta Chile Chico area. They have been described as unstratified, mainly angular gravel- and block-sized sediments of polymictic composition in a mixed matrix of sand, silt and clay (De La Cruz and Suárez, 2008) and form elongated to sinuous landforms located at topographic highs in this region.

https://doi.org/10.5194/egusphere-2023-2156
Preprint. Discussion started: 25 September 2023

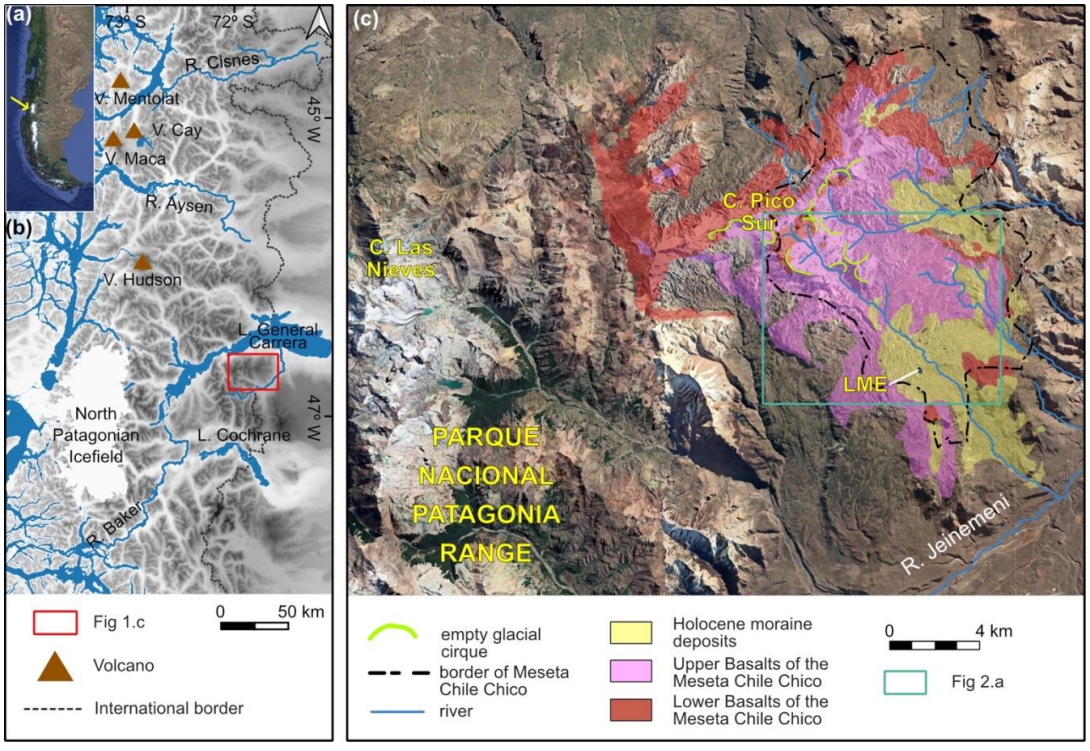

Figure 1 (a) Location of the North (yellow arrow) and South Patagonian Icefields in South America. Background corresponds to the Global Multi-resolution Terrain Elevation Data (GMTED 2010); (b) Location of the study site in Central Patagonia with location of volcanoes (V.) mentioned in the text. Background image corresponds to © Google Satellite (2023); (c) Main geological (De La Cruz and Suárez, 2008) and geomorphological units of Meseta Chile Chico (this work) with location of Laguna Meseta (LME). Other abbreviations: R.: rio; L.: lago; C.: cerro.

Another relevant geological feature of the Chile Chico Meseta is its proximity to volcanoes of the Southern Volcanic Zone (Futa and Stern, 1988), such as Hudson, Maca, Cay and Mentolat volcanoes (Fig. 1b). Several Holocene eruptions have been documented between Río Cisnes and Lago Cochrane (Stern et al., 2016; Weller et al., 2017) in surface deposits as well as in lake and fjord sediments. The most relevant of these events corresponds to the eruption of Hudson (H1) dated to between 8,530-7,750 cal yr BP. Most likely, this was the largest Holocene eruption for Central Patagonia (Naranjo and Stern, 2004).

https://doi.org/10.5194/egusphere-2023-2156
Preprint. Discussion started: 25 September 2023

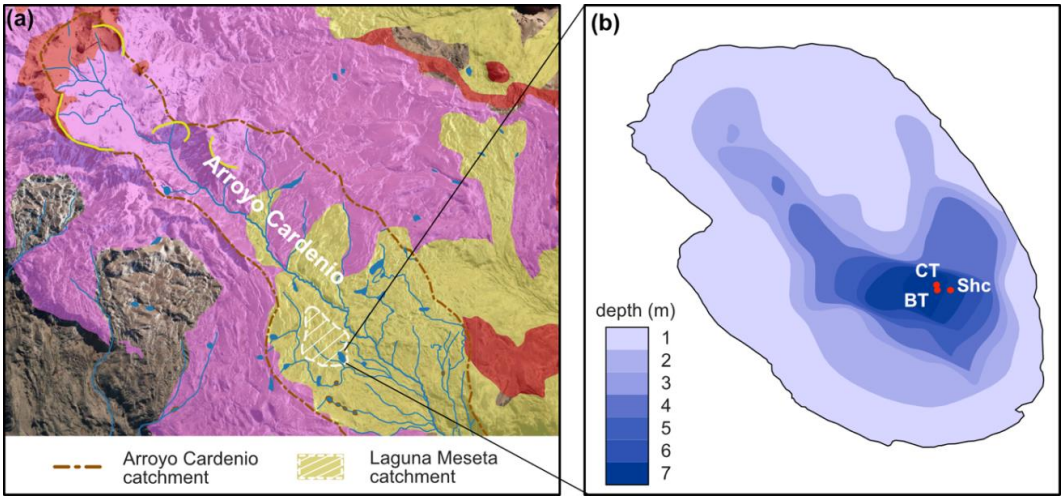

Figure 2 (a) Catchments of Arroyo Cardenio and Laguna Meseta (for location see blue frame of Fig 1.c). For colour signatures refer to Fig. 1.c. Background image corresponds to © Google Satellite (2023); (b) Bathymetry of Laguna Meseta and location of sediment cores LME–Shc, LME-BT and LME–CT.

2.2 Previous paleoenvironmental reconstructions

Moraine mapping and chronological studies at the eastern border of lakes General Carrera and Cochrane indicate that Meseta Chile Chico was located between two major ice lobes of the Large Patagonian Ice Sheet, which completely occupied these lake basins during the LGM (Caldenius, 1932; Glasser and Jansson, 2005) between ca. 34-16 ka (Bendle et al., 2017a; Douglass et al., 2005b; Singer et al., 2004; Smedley et al., 2016; Hein et al., 2010). Moreover, ages of post LGM moraines indicate that the General Carrera ice lobe remained at the northern border of the Meseta Chile Chico plateau at least until 14.7 ka (Smedley et al., 2016) before retreating further to the west to develop the General Carrera paleolake basin. Ice front reconstructions from the opening of the Baker valley surrounding the eastern border of the North Patagonian Icefield (Thorndycraft et al., 2019) point to a separation between the North Patagonian Ice Sheet and the ice cap that covered the Parque Nacional Patagonia around 12.6-10.5 ka (Glasser et al., 2016; Thorndycraft et al., 2019).

Reconstructions of the Patagonian Ice Sheet for our study site date its retreat from the eastern boundary of the Meseta Chile Chico to between 25-20 ka, but the ice cap that covered the Parque Nacional Patagonia remained active until 10 ka before splitting into the modern glaciers that occupy the catchment of this range today (Davies et al., 2020). Most of these reconstructions are based on moraine chronologies from the valleys and show a high confidence level for low altitudes, whereas for topographic highs, such as the studied Meseta Chile Chico, these reconstructions are not very precise. Therefore, the timing for deglaciation and consequent lake formation on Meseta Chile Chico remains unconstrained.

Moraine deposits in the vicinity of the North Patagonian Icefield dated to between 10-6 ka are scarce (Douglass et al., 2005a; Harrison et al., 2017; Sagredo et al., 2021). They indicate that during this period the Patagonian landscape was mainly formed by ice recession and splitting-up of this major ice sheet into several smaller glaciers covering regional topographic highs. Consequently, and as documented by several pollen records, large *Nothofagus* forests developed around Lago Cochrane supporting the existence of higher temperatures and/or higher effective moisture for this period (Villa-Martínez et al., 2012; Maldonado et al., 2022; Henríquez et al., 2017; Iglesias et al., 2018).

During the Middle Holocene between 6-4 ka, a period of glacial advances (Davies et al., 2020; Mercer, 1976; Glasser et al., 2004; Aniya, 1995) associated to the intensified activity of the Southern Hemisphere Westerly Winds (SWW, Kaplan et al.,

https://doi.org/10.5194/egusphere-2023-2156
Preprint. Discussion started: 25 September 2023

2016; Moreno et al., 2018) is documented for Western Patagonia. These conditions have been regionally identified in moraine deposits around the North Patagonian Icefield (Fernandez et al., 2012; Harrison et al., 2012; Nimick et al., 2016; Bertrand et al., 2012) and Cerro San Lorenzo in Central Patagonia (Sagredo et al., 2021; Sagredo et al., 2018), around the Southern Patagonian Icefield (Reynhout et al., 2019; Strelin et al., 2014; Kaplan et al., 2016), as well as in the Darwin Cordillera in South Patagonia (Reynhout et al., 2021) and in the northern Antarctic Peninsula (Kaplan et al., 2020). This stage could have also been responsible for a series of large dam-breaching events in several lakes of the Rio Baker and associated tributary valleys, as documented by dated glacial lake outburst flood (GLOF) deposits (Benito et al., 2021).

Similarly, moraine chronologies and historical records recognized from North to South Patagonia (Mercer, 1976; Glasser et al., 2005; Garibotti and Villalba, 2009; Davies and Glasser, 2012; Kaplan et al., 2016) suggest that the latest neoglacial advance occurred at ca. 0.5-0.2 ka (Davies et al., 2020), overlapping with the Late Holocene glacial period, commonly assigned to the Northern Hemisphere "Little Ice Age" (Grove, 2004). In opposition with records from the Northern Hemisphere, where this period has been documented as the strongest glacial advance for the Holocene, geomorphologic evidences in Patagonia indicate that it was of minor intensity in comparison with the Middle Holocene glacial advance (Glasser et al., 2005; Kaplan et al., 2016).

Although several studies on deglaciation and neoglaciation have been carried out at the borders of the North Patagonian Icefield (as well as in northern and southern areas of Patagonia) and in low altitudes such as regional valleys and lakes, the Meseta Chile Chico and its surrounding ranges have not yet been considered for paleoenvironmental studies.

3 Methods and Materials

3.1 Sediment coring and subsampling

In March 2020, one of the lakes from Meseta Chile Chico was sampled. It is unofficially referred to as Laguna Meseta (LME: 46.716º S, 71.844º W, 1,457 m a.s.l.) and belongs to the Arroyo Cardenio catchment system (Fig 2a). Three sediment cores with in total eight sections were collected at LME from the maximum water depth of 7 m at adjacent coring series (Fig 2.b). Cores LME-BT and LME-CT were extracted with a modified Livingston piston corer (diameter: 5 cm), whereas core LME-Shc was recovered with a UWITEC hammer corer (diameter 9.6 cm).

The cores were cut lengthwise by the lab team of the Center of Advanced Studies in Arid Zones - CEAZA (La Serena, Chile). One of the core halves remained at CEAZA for ongoing pollen analyses and the other was sent to the Geopolar lab (University of Bremen, Germany). In Bremen, core halves were described considering color (applying the Munsell Soil Color Charts), lithology, grainsize and pyroclastic fall-out deposits. After conservative (i.e., non-destructive) techniques such as downcore X-ray fluorescence (XRF) scanning, X-ray radiography as well as magnetic susceptibility logging were performed , a 3 m-long composite sediment record was constructed with the additional help of six visible tephra layers as marker horizons for correlation between core sections. Subsampling for additional parameters was carried out with 1-10 cm spatial resolution. All samples were immediately freeze-dried for further processing.

3.2 Geochemistry of tephra layers

Six tephra layers (labelled T1-T6 from bottom to top) were identified on the basis of macroscopic and microscopic (smear slides) sediment description as well as using radiographs and XRF core-scanning data. Due to their compositional variability, no element ratio correlates with all six tephra layers. Therefore, data points corresponding to these layers were discarded for correlation coefficient calculations.

From the basal section of the thickest (14.5 cm) tephra deposit, two bulk samples enriched in pumice were obtained. After freeze-drying, the samples were pulverized and fused with lithium tetraborate to produce glass beads that were analysed for

https://doi.org/10.5194/egusphere-2023-2156
Preprint. Discussion started: 25 September 2023

major and trace elements with wavelength dispersive X-ray fluorescence spectroscopy (Panalytical Axios^{max}) at the University of Oldenburg. Total Alkali Silica (TAS) diagram for tephra chemistry was plotted with the TAS template for Excel 1.1 (Stosch (2022).

3.3 XRF core scanning

Downcore X-ray fluorescence (XRF) scanning was performed on untreated core halves using the ITRAX XRF core-scanner (Croudace et al., 2006) at the GEOPOLAR lab (University of Bremen) with a Mo-tube that was run at 30 kV and 45 mA. A step size of 1 mm and a dwell time of 5 s per step were applied. This ensured average total count rates of approximately 50 kcps. To assure optimal data quality, a mathematical model (setting file) was fitted to a sum spectrum that contains all spectra recorded. Fitting was done with the ITRAX proprietary software Q-Spec (version 8.6.0). Element integrals (peak areas) were determined during batch processing using the designated setting file.

After assessing and cleaning the elemental data for outliers, five elements were selected for interpretation: Si, K, Ca, Ti and Sr. For these elements a centred log-ratio (clr) transformation (Weltje et al., 2015) was applied to avoid effects of intensity variability that may be caused by dilution effects of the different elements present in the sediment core. Downcore profiles are displayed as clr transformed element curves or as logarithmic elemental ratios. Running means were calculated with a moving window of 10 data points when possible, whereas for data gaps a linear interpolation was used instead. For organic matter (OM) content estimations, the logarithmic XRF incoherent/coherent ratio was applied (Guyard et al., 2007; Davies et al., 2015).

XRF results are presented as clr transformation (for single elements) or as natural logarithms (for ratios) throughout this publication.

3.4 Magnetic susceptibility

Magnetic susceptibility was measured at the Alfred Wegener Institute Helmholtz Centre for Polar and Marine Research in Bremerhaven, Germany. Measurements were carried out on half cores in 1 cm resolution on a Geotek Multi-Sensor Core Logger (Geotek Ltd, UK) using a Bartington MS2E sensor.

3.5 Grainsize

Grain size distributions were measured in 2 cm resolution (excluding tephra and other layers with high content of pyroclastic components) with a Beckman Coulter LS 200 laser granulometer. All samples were dried and homogenized prior to analysis. About 0.7 g of each sample was weighed into 50 ml centrifuge tubes. During pre-treatment, organic components were removed with a 30 % hydrogen peroxide solution at 105 °C. Biogenic opal (diatoms) was dissolved with a 2 mol/l sodium hydroxide solution at 85 °C. After being washed and centrifuged, the samples were shaken over night with a dispersion agent on a Na-polyphosphate base to ensure a proper dispersion of the grains. Each sample was treated with a sonication probe for 30 s directly before measurement and then measured for 60 s several times until three comparable replicates have been obtained.

3.6 Radiocarbon dating and age-depth modelling

A total of eight samples of bulk sediment were obtained (Table 2) at the CEAZA lab and sent to the Direct AMS laboratory (Washington State, US) for radiocarbon dating.

An age-depth model was obtained with rbacon (Blaauw and Christen, 2011) version 2.5.7 using the Southern Hemisphere calibration curve SHCal20 (Hogg et al., 2020). Deposits with tephra layers were modelled as slumps, as they represent episodes of instantaneous (event) deposition.

https://doi.org/10.5194/egusphere-2023-2156
Preprint. Discussion started: 25 September 2023

3.7 Bulk geochemistry

Loss on ignition (LOI) at 550º C was measured at the CEAZA laboratory with 1 cm intervals to determine OM. Total carbon (TC), total nitrogen (TN) and total sulphur (TS) were measured every 5 cm additionally, whereas total inorganic (TIC) and total organic (TOC) carbon percentages were measured only every 10 cm with a CNS elemental analyser (EuroEA) at the Geopolar lab (University of Bremen).

Additionally, biogenic silica (BiSi) was measured in 2 cm steps at the Geopolar lab using the automated leaching method (Müller and Schneider, 1993).

3.8 Compiled chronologies

Published cosmogenic and optically stimulated luminescence (OSL) ages cited throughout this work are presented as their means in ka calculated by Davies et al. (2020) after being reviewed in their original publication. Radiocarbon ages published prior to the publication of the SHcal20 calibration curve (Hogg et al., 2020) were recalibrated. Cosmogenic and OSL chronologies, as well as time periods defined by a mix of different dating techniques are always presented in "ka".

4 Results

4.1 Lithology

By means of macroscopic description as well as magnetic susceptibility (MS) and grainsize analysis, the lithology of the LME composite profile (LME-CP) was grouped into nine lithological units (Units A-H and T5), of which two (F, T5) are dominated by tephra deposition (Fig. 3).

For the whole composite profile, the biogenic content is characterized by plant remains, lenses of OM and diatoms, which are significantly more abundant within silty lithological units H to D. Similarly, glass shards are observed in all lithological units but particularly abundant in units G and B. Glass, pumice and obsidian fragments between 0.5 and 1-mm size as well as fragmented crystals of pyroclastic origin are found throughout and mixed with the sediment.

The lowermost sediments of LME-CP are very dark greyish brown silts that form unit H (292.5 to 240.5 cm composite depth). This unit is mainly composed of laminated organic (diatomaceous) sediments with abundant traces of mm-sized plant remains and dark grey lenses of OM.

Unit G (240.5-229 cm composite depth) is made of dark greyish brown, clayey to silty very fine sand with plant remains. Unlike the other boundaries between sedimentological units, the boundary between units H and G is sharp. Nevertheless, we do not interpret this boundary as an erosional surface. Instead, we attribute the change in sediment properties between these two units to the abundance of glass and crystalline fragments (quartz and feldspars) from tephra layer T6, whereas lacustrine sediments remain the main component.

Unit T5 (229-214.5 cm composite depth) corresponds to a 14.5 cm thick pyroclastic layer and therefore is defined as a lithological unit, but not considered for environmental interpretation. Because of thicknesses <1.7 cm, the remaining tephra layers (T1-4 and T6) are not defined as lithological units. The tephra record is addressed in more detail in the following subsection.

Between 214.5 and 199.6 cm composite depth, Unit F lies immediately on top of T5. This unit corresponds to a distinctly laminated section, formed by layers of vitric ash that alternate with mixed layers of ash and clay. Because the major component of this section is pyroclastic material, together with the deposit assigned to T5, Unit F is also excluded from the age/depth model.

https://doi.org/10.5194/egusphere-2023-2156
Preprint. Discussion started: 25 September 2023

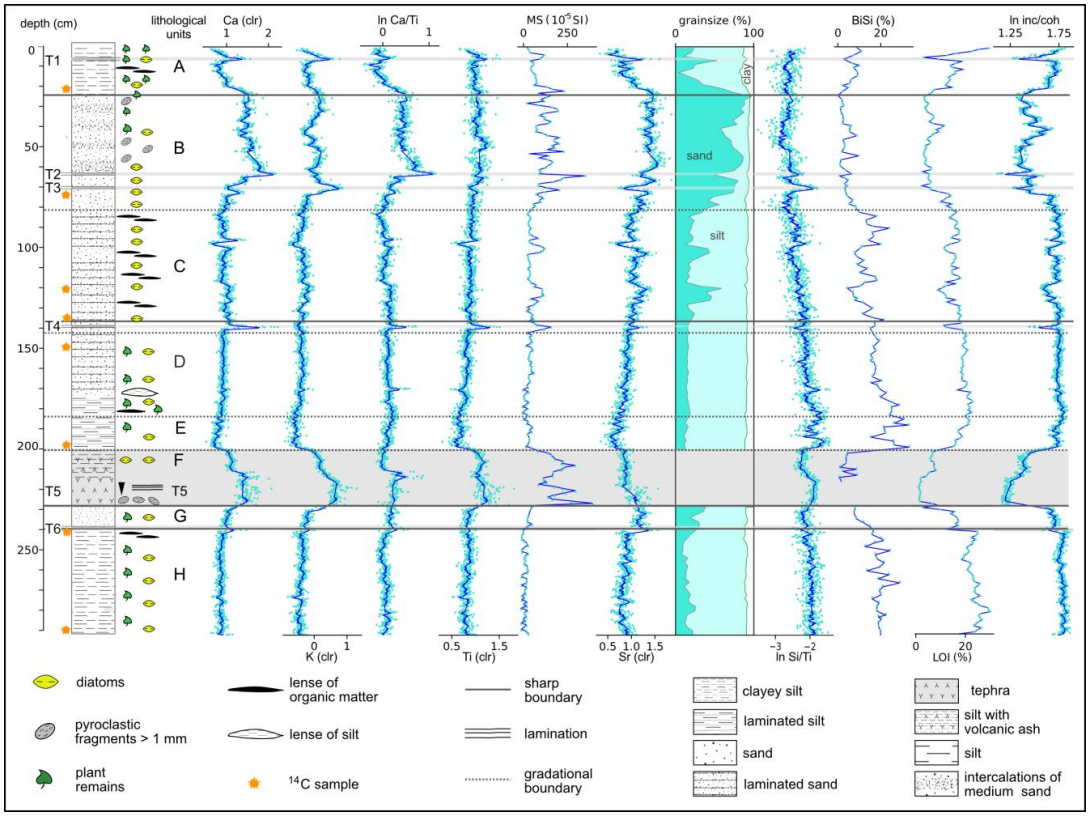

Figure 3 Lithology, sedimentary structures, lithological units, and main elemental components (clr values and logarithmic ratios) with data points (light blue dots) and running means (dark blue lines), magnetic susceptibility (MS), grainsize, biogenic silica (BiSi), loss on ignition at 550 °C (LOI) and the logarithmic incoherent-coherent ratio (inc/coh) of the composite sediment record vs depth.

Unit E (199.6-184 cm composite depth) includes very dark to dark greyish brown silt beds with intense lamination of dark grey and brown layers (1 to 3 mm-thick). Lamination becomes less pervasive and thinner towards the top. Plant remains and organic lenses as well as lenticular beds of light brown silt are recognized.

Unit D is formed by very dark brown, laminated sandy silt to silt and ranges from 184 to 139.7 cm sediment composite depth. This unit also contains high amounts of organic components, but unlike Unit C does not present intercalations of medium sand.

Unit C is overall enriched in organic components, plant remains and dark brown lenses of OM. It ranges from 139.7 to 78.6 cm composite depth and is a transitional unit between units D and B. It is formed by very dark brown, diffusely laminated sandy silt to clayey silt with irregularly intercalated beds of sublithic fine sand.

Unit B (78.6-24.1 cm composite depth) is composed of very dark greyish brown, fine to very fine sublithic sand, with intercalated 0.5 to 2 cm-thick beds of medium to coarse, subarcosic sand. Its composition is highly minerogenic with subangular quartz and feldspar as main (mafic) volcanic lithics as secondary components. Micaceous minerals, felsic volcanic clasts, unrecognized lithic clasts, and plant remains are subordinated. Grainsize is very well sorted and some lenses of very fine sand are observed. Near to its top, grainsize decreases progressively and the transition to unit A is gradual.

Finally, Unit A spans the upper 24.1 cm of the profile and is composed of dark yellowish brown sandy to clayey silt with millimetric plant remains. Lenses of light brown clay (1 cm thick) and dark brown lenses of OM are also observed.

https://doi.org/10.5194/egusphere-2023-2156
Preprint. Discussion started: 25 September 2023

4.2 Tephra records and tephrochronology

The profile LME-CP contains six tephra layers (T6 to T1, Fig. 3). T5 is the most prominent one with a thickness of 14.5 cm, whereas the other five tephra layers have thicknesses that range between 8 and 17 mm. XRF scanning results show a non-uniform composition of these layers, reflecting different volcanic sources. T2 and T4 are enriched in Ca and poor in K, T3 shows the opposite trend, whereas T1, T5 and T6 are enriched in Ca and K, while Ti is enriched for T1, T4 and T5 (Fig. 3). Within LME-CP T5 stands out for its thickness and a vitric laminated lapilli deposit (fragments > 2 mm) at the base, which grades into ash-sized pyroclastic fragments and elongated brownish glass shards. In its upper part, T5 represents distinct laminations marked by alternating coarse and fine ash layers.

Table 1 Major element composition (all values as wt%) for Hudson H1 bulk samples from the Lago Cochrane area (Stern et al., 2016) and from Meseta Chile Chico (this work).

Lago Cochrane area										
sample name	**SiO_2**	**TiO_2**	**Al_2O_3**	**Fe_2O_3**	**MnO**	**MgO**	**CaO**	**Na_2O**	**K_2O**	**P_2O_5**
94t-44	62.15	1.41	16.24	4.97	0.16	1.69	3.65	5.60	2.57	0.32
Meseta Chile Chico										
CT3 120-145	55.57	1.40	15.80	7.03	0.16	2.63	4.87	4.74	1.74	0.48
CT3 95-120	56.90	1.44	15.33	7.21	0.17	2.56	4.40	4.80	1.92	0.51
average values (this work)	56.24	1.42	15.57	7.12	0.16	2.60	4.64	4.77	1.83	0.49

According to our age model, the age of T5 ranges between 8,987 and 8,018 cal yr BP with a mean age of 8,277 cal yr BP. This age suggests a likely correlation with tephra records from Mentolat (Men1) and Hudson (H1) volcanoes (Fig 1.b, (Naranjo and Stern, 1998, 2004; Stern et al., 2016). Nevertheless, thickness and petrography represent larger similarities with tephra layers corresponding to the H1 rather than to the Men1 eruption (Table 1, Fig. 4).

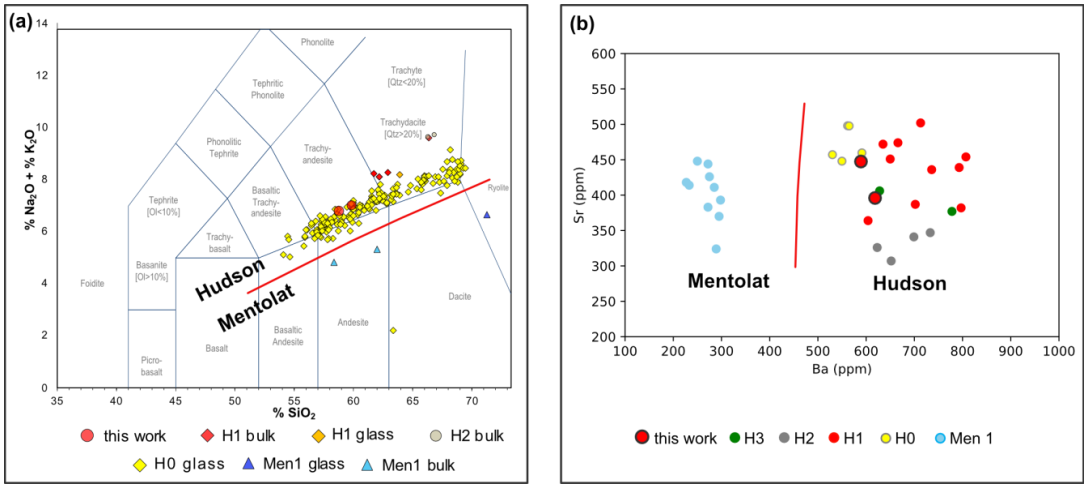

Figure 4 (a) Total Alkali Silica (TAS) volcanic classification diagram (Bas et al., 1986) and b) Sr vs Ba concentrations for tephra layers identified around Lago General Carrera and Lago Cochrane from Hudson and Mentolat volcanoes. (H0: Bendle et al., 2017a; H1: Naranjo and Stern, 1998, Stern et al., 2016; Men 1: Naranjo and Stern, 2004, Stern et al., 2016; H2, H3: Stern et al., 2016).

https://doi.org/10.5194/egusphere-2023-2156
Preprint. Discussion started: 25 September 2023

For H1 an age range between 8,585 and 8,200 cal yr BP (mean age of 8,415 cal yr BP, Stern et al. 2016) was previously documented for the catchment of Lago Cochrane (Maldonado et al., 2022; Naranjo and Stern, 1998, 2004; Stern et al., 2016) and the Rio Zeballos valley (Mcculloch et al., 2017), while studies located between Lago Cochrane and Río Cisnes date the Men1 eruption to between 7,864 and 7,399 cal yr BP (Stern et al., 2016; Naranjo and Stern, 2004).

Geochemical analysis performed in this study indicates that T5 has an average andesitic composition (Table 1). Elemental percentages are slightly lower than published concentrations for H1 (Fig 4a). These lower values likely are influenced by sample treatment, which in this study did not include the removal of the sediment matrix before analysis. Therefore, our samples probably are "less enriched" in Si, K and Na compared to cleaned pyroclastic samples. Nonetheless, they still fall within the field of alkali-enriched magmatism (Fig. 4a) that distinguishes the Hudson volcano from other eruptive centres of the Southern Volcanic Zone such as the Mentolat Volcano (Futa and Stern, 1988; Lopez-Escobar et al., 1993; Stern, 1991).

To confirm our classification, we compare the trace element composition of volcanic products from Hudson and Mentolat volcanoes. Our results show that the sampled layers are chemically consistent with pyroclastic deposits (Bendle et al., 2017b; Naranjo and Stern, 1998, 2004; Stern et al., 2016) and volcanic rocks from the Hudson volcano (Fig 4.b), which are characterized by a high Ba/Sr ratio (Stern, 1991, 2008). In contrast, concentrations of Ba for the deposits of Men1 are significantly lower (Naranjo and Stern, 2004; Stern et al., 2016). In agreement with the latter, we assigned T5 to the H1 eruption of the Hudson Volcano (Naranjo and Stern, 1998; Stern, 1991).

4.3 Siliciclastic elemental composition, grainsize and magnetic susceptibility

The highest values of the selected elements Ca, K and Ti, are found at T5 and Unit F. These peaks, as well as the smaller ones for T1-T4, are related to a high content in volcanic glass and/or crystals (Fig. 3).

The lowermost Units H, G, E and D show very low values of elemental concentrations. Consequently, they exhibit high values for OM represented by the inc/coh ratio. In the case of Unit G, the slightly higher values for Ca, Ti and K are most likely associated to a high content of crystalline components accumulated in this unit by reworking of T6. Therefore, this increase is not associated to environmental influences.

Throughout Unit C, element concentrations progressively increase until Unit B. Although the chemical composition at the base of Unit B is obscured by T3 and T4, it is still observable that values for chemical elements reach their maximum and remain high in the sediments above the tephra layers, while inc/coh reaches a minimum.

In Unit A elemental concentrations drop once again to minimum values (except for T1) with a stepwise increase in inc/coh.

As expected, MS tendencies are similar to elemental concentrations throughout LME-CP, as its maximum values are found in tephra layers (T1-T6) and Unit F. Grainsize measurements, which were not performed along tephra layers and Unit F, have maximum values in highly minerogenic Unit B. Minimum values for MS and finer grainsize percentages are found at the base of the core. Unit C peaks with sand content, which correlates well with MS, and both parameters increase until their maximum in Unit B. They drop synchronously at the contact between Units B and A.

4.4 Organic Proxies

TN and TS concentrations are below 1.7 % and 0.3 %, respectively, while TIC percentages, considered as estimation of carbonates, are below 1 % for all measured samples. Hence, the presence of nitrogen, sulphur and carbonates in the sediments is negligible. Consequently, TOC and TC percentages are almost identical confirming that the carbon content of the samples originates primarily from OM. LOI 550º C analyses show a high degree of agreement ($R^2 = 0.92$, Fig 5.a) with TC ≈ TOC values, reflecting that LOI results are a reliable indicator for organic matter of the sediments.

The high correlation of the inc/coh ratio with LOI550 ($R^2 = 0.87$, Fig. 5.b), indicates that inc/coh ratios derived from XRF core-scanning with 1 mm spatial resolution can be used as a proxy for organic matter content as has been shown for other lacustrine sediments (Davies et al., 2015; Guyard et al., 2007; Burnett et al., 2011).

https://doi.org/10.5194/egusphere-2023-2156
Preprint. Discussion started: 25 September 2023

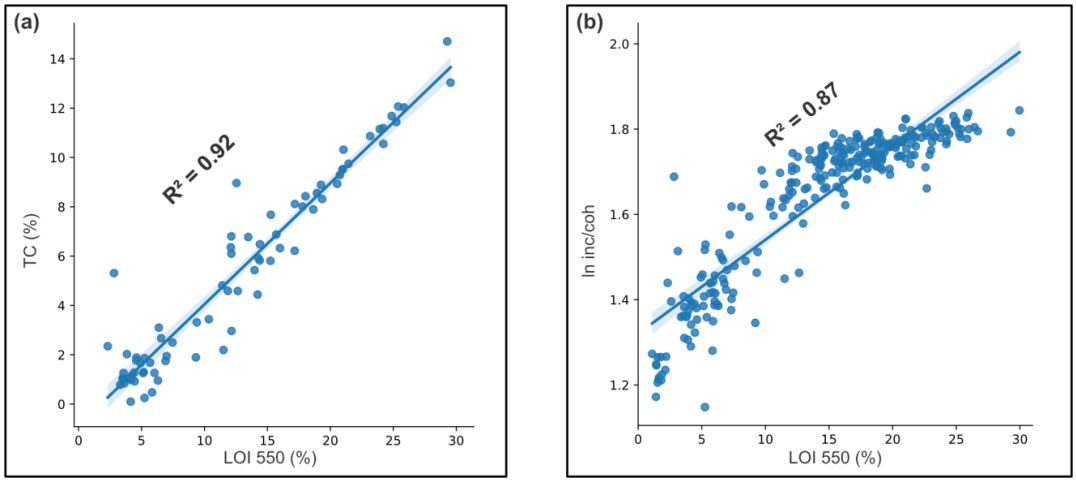

315 Figure 5 (a): Covariance plots with R^2 values for TC vs LOI 550° C and (b) for inc/coh vs LOI 550° C.

As expected, LOI and BiSi reach their minimum in units T5 and F, as well as with identified tephra layers. Furthermore, allochthonous proxies increase towards Unit B, while organic proxies display opposite trends (Fig. 3). LOI percentages show a moderate decrease from the bottom of LME-CP to the base to Unit B (except for low values within the crystal-bearing
320 Unit G). At Unit B they reach lowest values and abruptly increase again at the base of Unit A towards the surface. Maximum values are found in Unit H and in surface sediments (Unit A).

4.5 Chronology

Eight radiocarbon dates were obtained and applied for age/depth modelling (Table 2, Fig. 6). The mean calibrated ages range
325 between 613 and 9,883 cal yr BP and consistently increase with depth. Therefore, all ages were considered for calculation of the age/depth model.

Table 2 AMS radiocarbon dates from Laguna Meseta.

core section	section depth (cm)	composite depth (cm)	Sample code	sample type	Radiocarbon age (^{14}C BP± 1σ)	calibrated mean (cal yr BP)
shc	20.5	20.5	D-AMS 043184	sediment (bulk)	730 ± 18	613
shc	71	71	D-AMS 043185	sediment (bulk)	4555 ± 27	5092
shc	117	117	D-AMS 043186	sediment (bulk)	5737 ± 26	6509
CT2	86	130.4	D-AMS 043187	sediment (bulk)	6208 ± 26	7050
CT3	8.5	141	D-AMS 043188	sediment (bulk)	6499 ± 29	7336
CT3	65	198	D-AMS 043189	sediment (bulk)	7261 ± 42	8257
CT4	21.5	240.5	D-AMS 043190	sediment (bulk)	8579 ± 35	8721
CT4	71.5	290	D-AMS 043191	sediment (bulk)	8869 ± 32	9883

330

Additionally, T5 assigned to the Hudson H1 eruption is used as a temporal control point for the ^{14}C-based age/depth model. The 14.5 cm of sediment above T5 (Unit F, Fig 3) correspond to remobilization of H1 fall-out deposits in the lake catchment and are considered as contemporaneous to this eruption and, therefore, modelled as one instantaneous event. The published

https://doi.org/10.5194/egusphere-2023-2156
Preprint. Discussion started: 25 September 2023

age of H1 (mean age: 8,415 cal yr BP, age range in lacustrine cores: 8,585-8,200 cal yr BP; Stern et al., 2016) agrees with our radiocarbon chronology, which provides an age range between 8,987 and 8,018 cal yr BP for T5.

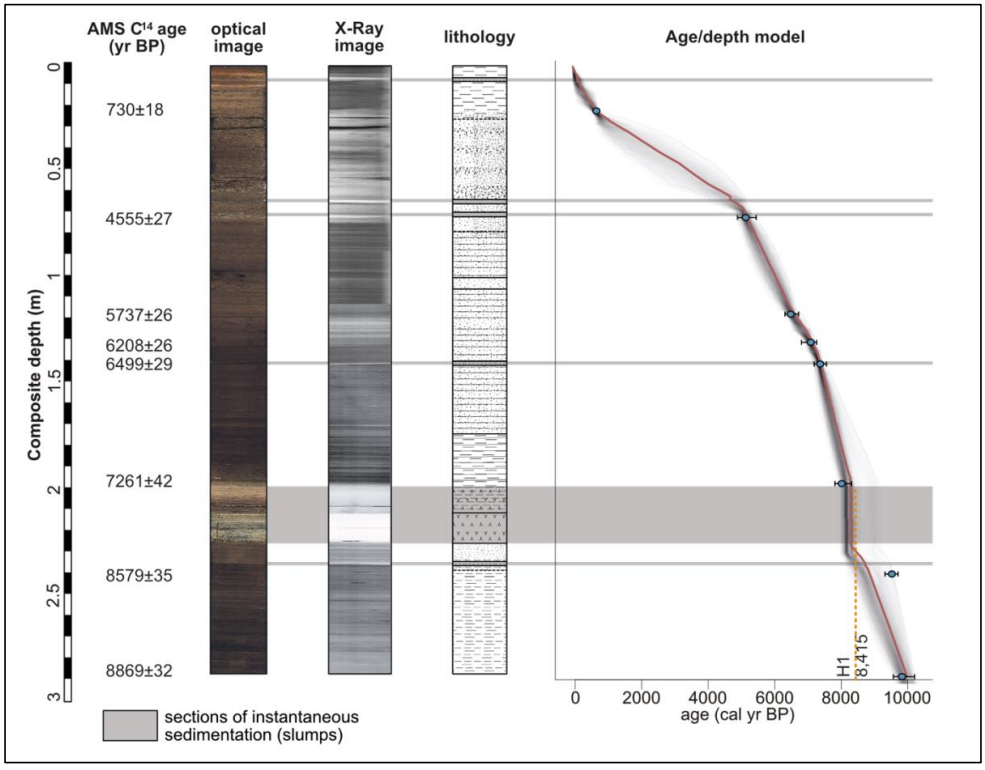

Figure 6 Radiocarbon ages, optical photography, radiography, lithology, and age/depth model of the composite sediment record for LME. Vertical orange line marks the mean age for the Hudson H1 tephra (Stern et al., 2016). The age/depth model was developed with the rbacon software 2.5.7 applying the southern hemispheric calibration curve SHCal20 (Hogg et al., 2020). Symbols for lithological patterns are displayed with Figure 3.

The radiocarbon age of 8,721 cal yr BP from 240.5 cm composite depth (D-AMS 043190, Table 2) seems to be slightly too old compared with our age-depth model, but it is partly still within the error of this model. We think that this offset does not contradict our chronology and that it might be related to older material within the bulk sample, which was previously remobilized by bioturbation. Another possible explanation could be that our age model overestimates the timespan of H1, since lacustrine fall-out deposits and settling of reworked tephra from the same eruption can occur with a century-long delay (Boygle, 1999). Therefore, lithological Unit F and T5 might not have been completely synchronous. Nevertheless, this age has no large effect on our age/depth model and, therefore, it was not excluded from the chronology.

5 Interpretation

5.1 Proxy Analysis

The high correlation of Ca, Ti, K and Sr for LME-CP (Fig. 7.a) are compatible with geochemical data of the Meseta Chile Chico basalts (De La Cruz and Suárez, 2008; Espinoza et al., 2005) pointing to these geological formations as the main source of clastic sediment components.

https://doi.org/10.5194/egusphere-2023-2156
Preprint. Discussion started: 25 September 2023

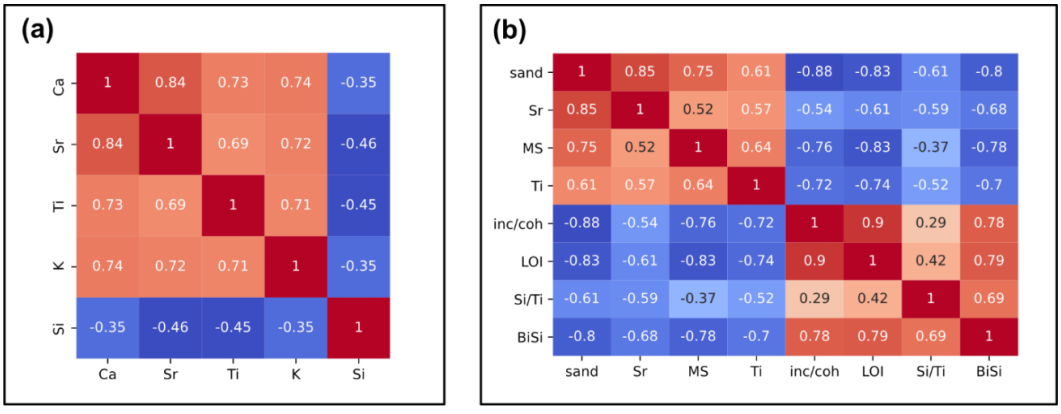

Figure 7 Correlation matrix for (a) elemental clr values (n=2,719) and (b) selected proxies (n=146).

Ti (commonly used as proxy for catchment erosion, Davies et al., 2015) correlates well with MS (R=0.64, Fig 7.b). We associate this correlation to Ti-Fe oxides such as ilmenite and magnetite present in the groundmass of Meseta Chile Chico basalts (Espinoza et al., 2005) and consequently, we interpret Ti values as proxy for influx of (chemically) unweathered basalt clasts from the catchment.

Similarly, we found a strong match between Sr and sand percentages (R=0.85), indicating that the sand fraction is enriched in Sr. We attribute this to high concentrations of Ca-minerals (feldspars), since Ca and Sr (R = 0,84) are usually components of the same mineralogy with the exception that Ca is also related to most tephra layers (only T3 is depleted in Ca) and mixture of glass components with the sediments, whereas Sr is depleted in most volcanic ashes. For this reason, we choose Sr instead of Ca as a proxy for Ca-bearing silicates.

To assess the source variability of allochthonous sediments, we use the Ca/Ti ratio. We observe that this ratio remains mostly invariable between Units H and C (except for Unit T5). Thus, the source of siliciclastic material remained constant from the base of LME-CP upwards to 60 cm composite depth. Similar to the Sr values, high Ca/Ti ratios (Fig. 3) between 60 and 25 cm suggest that the source of Ca for this section is more related to Ca-silicates, most likely Ca-feldspars rather than to remobilization of fall-out deposits of T2 (enriched in Ca, according to our XRF data).

We also compare the proxies for minerogenic components (Ti, Sr, Ca/Ti) with the minerology of Unit B, where allochthonous parameters reach their maximum. The minerogenic composition of LME sediments, as observed for its sandy fraction, reflects high concentrations of sand-sized clastic material, such as quartz, feldspars and dark (mafic) volcanic lithics. This correlates well with the insights presented above and validates our chosen ratios for allochthonous proxies.

Organic proxies LOI, inc/coh and BiSi also show strong correlations amongst them (R=0.69-0.9, Fig. 7.b). Furthermore, to evaluate the overall Si content of the sediments, we tested Si/Ti as a proxy for BiSi percentages (Melles et al., 2012) and determined a good link between both parameters (R = 0.69). This documents that elemental Si variations with depth are mostly influenced by diatom accumulation, although siliciclastic detritus including pyroclastic fragments occur to a lesser degree.

5.2 Holocene paleoenvironmental evolution of Meseta Chile Chico

To evaluate the change of depositional conditions we plotted selected proxies vs time (Fig. 8). Ca/Ti, Ti and Sr, which represent detrital source variability, basaltic input, and sand-sized clastic supply, respectively, are considered as indicators for allochthonous input. Based on the significant correlation with BiSi as well as with LOI (Figs. 3, 5.b and 7.b), we interpret the inc/coh ratio as an indicator for lacustrine productivity (Fig. 8). Variability of these proxies during the last 10,000 years suggests four major stages of lacustrine sedimentation.

https://doi.org/10.5194/egusphere-2023-2156
Preprint. Discussion started: 25 September 2023

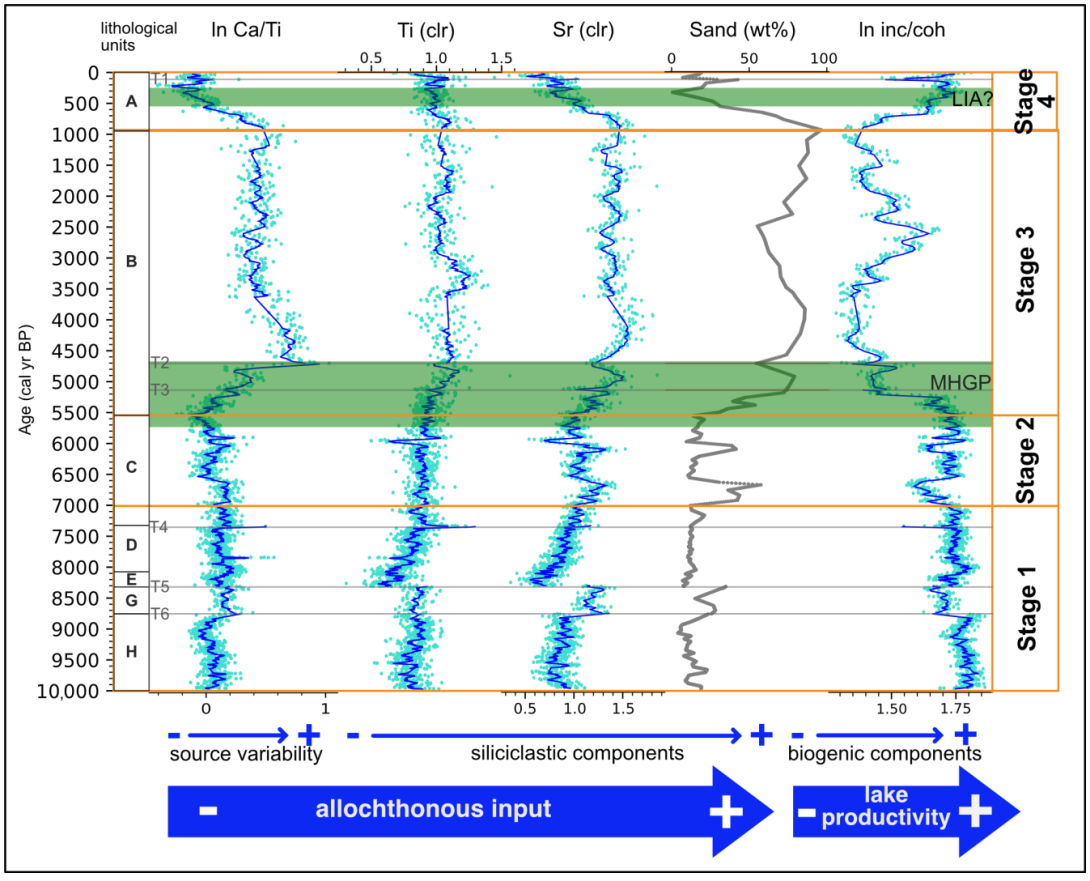

Figure 8 Lithology, running mean (dark blue line) and raw data (light blue dots) for selected element ratios, sand content and inc/coh ratio vs age and their interpretations for the LME sediment record. Grey lines indicate instantaneous events of tephra deposition. The Mid-Holocene glacial period (MHGP) according to glacier chronologies within our study area (references at Fig. 10) and the Little Ice Age (LIA) are marked.

The oldest stage recorded (Stage 1) started at least 10,000 years ago. It is characterized by high lacustrine productivity with a decreasing trend. Consequently, allochthonous proxies have low values but increase slowly along Stage 1. This trend is interrupted around 7,000 cal yr BP, with a sudden increase of allochthonous proxies between 7,000 and 6500 cal yr BP, and between 6200 and 5900 cal yr BP. Rising values of Ti point to the Meseta Chile Chico basaltic units (Fig 1.c) as the main detrital source of the sediments. Small variations in the Ca/Ti ratio are likely due to the presence of pyroclastic materials (reworked from T4, T5 and T6, Fig 6) rather than changes in detrital provenance. Accordingly, we interpret Stage 1 as a relatively stable period of high lacustrine productivity until 7,000 cal yr BP, when this development was interrupted by short periods of higher clastic supply from the catchment, marking the beginning of Stage 2 and the transition into the completely different environmental conditions of Stage 3 (Fig. 8).

An abrupt increase in terrigenous components takes place at ~5,500 cal yr BP, setting the start of Stage 3. An enhanced deposition of terrigenous material dilutes biogenic production, causing organic components to drop as documented by a decreasing inc/coh ratio.

https://doi.org/10.5194/egusphere-2023-2156
Preprint. Discussion started: 25 September 2023

Besides an exceptional peak of organic components around 2,500 yr cal BP, Ti values indicate that detrital supply peaked at ~3,400 cal yr BP and remained relatively high with some oscillations throughout the entire Stage 3. Sand percentages and Ti show an overall high correlation for the Early Holocene, but start to diverge after 4,700 cal yr BP. At 1,000 cal yr BP sand-sized components and Sr values reach their maximum. These differences together with the geological setting of the Meseta Chile Chico points to a concentration of Ca(Sr)-feldspar minerals within the sand fraction caused by stronger erosion of Meseta Chile Chico basalts or by a change in the main detrital source from the alkali enriched Upper Basalts to the more mafic (non-alkaline) Lower Basalts of the Meseta Chile Chico. This suggest that the catchment of LME might have extended into the ridge that connects Meseta Chile Chico and Cerro Las Nieves (Fig 1.c) during this stage.

Around ~800 cal yr BP, terrigenous supply starts to decrease, and autochthonous lacustrine deposition (inc/coh ratio) predominates again, setting the start of Stage 4 and indicating a major change in sediment supply. Sand percentages decrease, while clay slightly increases (Fig. 3). At ca. 400 cal yr BP, biogenic components reach the maximum of Stage 4 (meanwhile siliciclastic components reach their minimum around 400-300 cal yr BP) and remain at high values until present times, since proxy peaks at ~50 cal yr BP are related to T1 remobilization and not to changes in paleoenvironmental conditions. This probably adds to a higher lacustrine productivity and points to a waning of runoff during the last millennium.

6 Discussion

6.1 Holocene paleoenvironmental evolution of the Meseta Chile Chico

Available chronologies of post LGM moraines (Fig. 9) in the vicinity of Meseta Chile Chico indicate that the Patagonian Ice Sheet must have retreated from surrounding valleys at 17.1-12.7 ka between latitudes 46-48º S (Boex et al., 2013; Davies et al., 2018; Smedley et al., 2016; Turner et al., 2005). However, radiocarbon ages of deglaciation of regional lakes are younger than those indicated by their nearby moraine chronologies. Lake cores from Río Cochrane valley indicate that lacustrine sedimentation begun at 11,500 cal yr BP (Maldonado et al., 2022), meanwhile moraine studies in the nearby area indicate ages between 16.5-15.6 ka (Boex et al., 2013; Turner et al., 2005) for ice retreat. We attribute this difference to the temporal gap between glacier recession and the subsequent beginning of organic sedimentation in lacustrine basins. Additionally, recent studies on glacial lake outburst floods date the opening of the valley of Río Baker, the event that separated the Parque Nacional Patagonia icefield from the Patagonian Ice Sheet, to around 12.8 ka (Benito and Thorndycraft, 2020; Thorndycraft et al., 2019). The only available environmental reconstructions for the Parque Nacional Patagonia icefield correspond to two moraine ridges near Fachinal (30 km NW of our study site) with mean exposure ages of 8.2 and 6.2 and an estimated paleo-equilibrium line altitude (paleo-ELA) of ~1,100 m a.s.l. for these time intervals (Douglass et al., 2005a). However, there is large scatter as ages from two neighbouring recessional moraines, i.e. 20.3-9.4 ka for the older moraine and 11-5.8 ka for the younger moraine, were treated individually rather than using a calculated mean (Davies et al., 2020). Our results show that at ca. 10,000 cal yr BP (minimum age for the formation of LME at 1,457 m a.s.l.) the paleo-ELA was already above 1,460 m a.s.l. and remained above this altitude throughout the Holocene. In consequence, we consider the maximum age of 20.3 ka for the ~1,100 m a.s.l. paleo-ELA as a maximum age for deglaciation of the Parque Nacional Patagonia Range and Meseta Chile Chico topographic high, indicating that the Laguna Meseta originated between 20 and 10 ka. The timing of Laguna Meseta, its altitude, and location with respect to the 10 ka paleomargins of the Parque Nacional Patagonia icefield (Davies et al., 2020), suggest that the formation of this lacustrine basin might be associated to either paraglacial or periglacial processes.

The deglaciation reconstructions indicate a glacier retreat for the Early Holocene (11.5-8.0 ka), which triggered the drainage of several major regional lacustrine basins, such as Lago General Carrera, Lago Cochrane and the Tranquilo paleolake (Fig. 10.a, Benito et al., 2012). Furthermore, the expansion of *Nothofagus* forests along the Chacabuco and Baker valleys and in the Lago Cochrane area (Villa-Martínez et al., 2012; Iglesias et al., 2018; Henríquez et al., 2017; Maldonado et al., 2022) for this period (Figs. 10d-e), points to more temperate or wetter environmental conditions. These correlate well with the maximum

https://doi.org/10.5194/egusphere-2023-2156
Preprint. Discussion started: 25 September 2023

rates of lacustrine production documented by Stage 1 of LME. For the same time, moraine deposits are documented at ca. 9.5 ka for Laguna San Rafael (Harrison et al., 2012), at 9.8-6.7 ka at Cerro San Lorenzo (Sagredo et al., 2021) and at 11-5.8 ka at Fachinal (Fig 9, Davies et al., 2020; Douglass et al., 2005a). Nonetheless, these chronologies are either too scattered or they only represent local glacier advances to be regarded as regional glacial stages, explaining why they are not documented at Meseta Chile Chico.

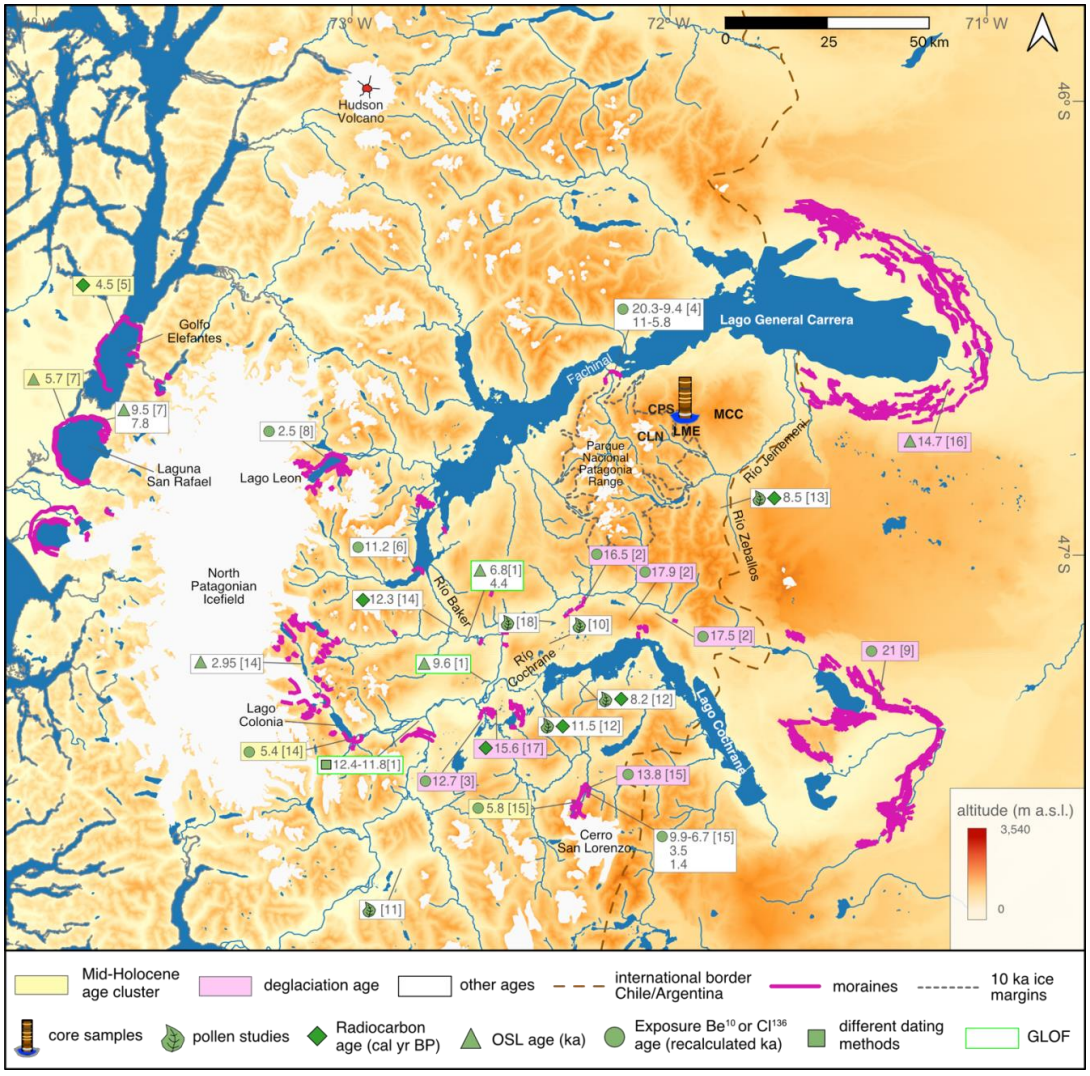

Figure 9 Ice retreat chronologies for the area east of the North Patagonian Icefield with the type of dating indicated. Lakes, ice cover, ice paleomargins, river and moraines were taken from Davies et al., 2020. GLOF: glacial lake outburst flood. Numbers given in brackets refer to the source publications: [1] Benito et al., 2021; [2] Boex et al., 2013; [3] Davies et al., 2018; [4] Douglass et al., 2005a; [5] Fernández et al., 2012; [6] Glasser et al., 2012; [7] Harrison et al., 2012; [8] Harrison et al., 2008; [9] Hein et al., 2010; [10] Henriquez et al., 2017 ; [11] Iglesias et al., 2018; [12] Maldonado et al., 2022; [13] McCulloch et al., 2017; [14] Nimick et al., 2016; [15] Sagredo et al., 2018, 2021; [16] Smedley et al., 2016; [17] Turner et al., 2005; [18] Villa-Martinez et al., 2012.

https://doi.org/10.5194/egusphere-2023-2156
Preprint. Discussion started: 25 September 2023

In contrast, the development of periglacial conditions above ca. 1,000 m a.s.l. documented by pollen studies from the Río Zeballos valley (Fig. 9) between 7,500-6,500 cal yr BP (McCulloch et al., 2017) is synchronous with the increase of sand at 7,000 cal yr BP that marks the beginning of Stage 2 at LME. This is pointing to wetter and/or colder climatic conditions. Records of paleovegetation at lower altitudes around the North Patagonian Icefield do not show periglacial evidence (Iglesias et al., 2018; Villa-Martínez et al., 2012). Moreover, Laguna Anónima documents an increase of *Nothofagus* at this time (Maldonado et al., 2022). In consequence, we associate the periods from 7,000-6,500 cal yr BP and from 6,200-5,900 cal yr BP with high sand/silt sedimentation to more humid conditions rather than to lower temperatures. These periods represent constrained events that are recorded only at higher and environmentally more sensitive areas.

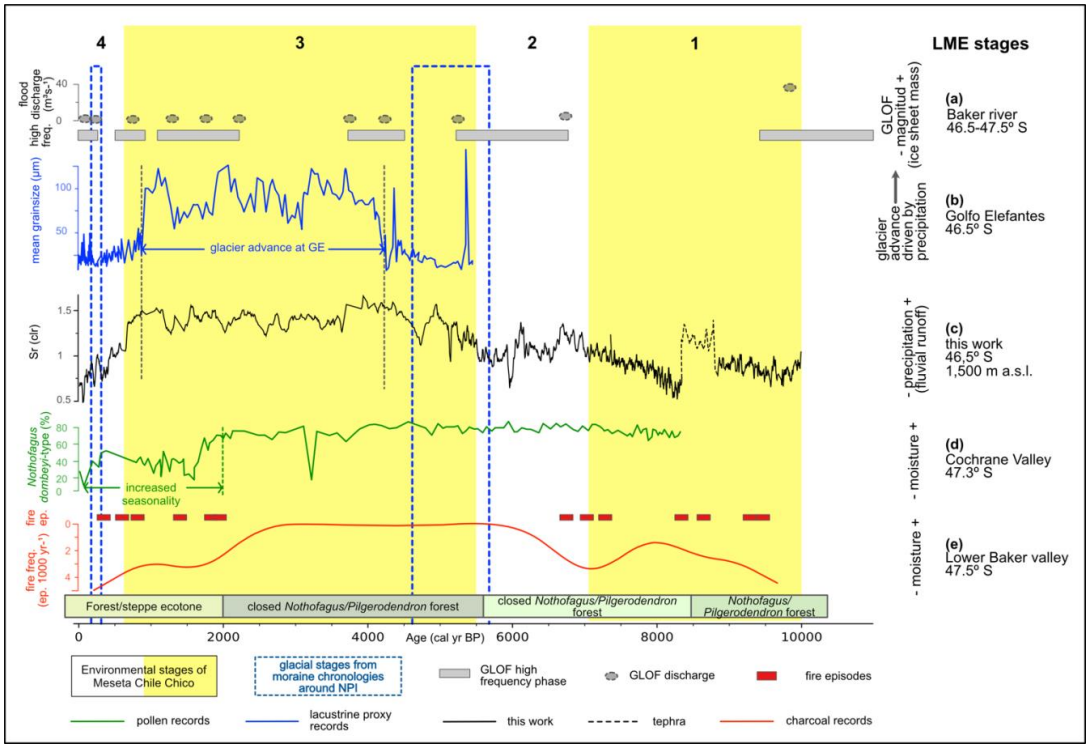

Figure 10 Selected proxies from LME in comparison to local records. (a) Glacial lake outburst flood (GLOF) magnitude and phases of high frequency (Benito et al., 2021). (b) Mean grainsize values at Golfo Elefantes (Bertrand et al., 2012) indicating an advancing Gualas glacier. (c) Sr (clr) values as proxy for fluvial runoff at Meseta Chile Chico. (d) *Nothofagus Dombeyi*-type tree pollen percentages from lacustrine records of the Lago Cochrane Valley as proxy for moisture/precipitation (Maldonado et al., 2020). (e) Pollen zones, fire frequency (number of fires per 1,000 years) and fire episodes at Lower Baker Valley (Iglesias et al., 2018). Stages from Fig. 8 (white yellow bands) and neoglaciations around the North Patagonian Icefield (squares with dashed blue lines) are also displayed. Ep.: Episodes; Freq.: frequency.

Contrarily, the younger Middle to Late Holocene (ca. 6-0.2 ka) moraine dates show active advances and retreats of the ice cover throughout Central and South Patagonia (Davies et al., 2020; Glasser et al., 2005; Reynhout et al., 2021). The transition from autochthonous to allochthonous deposition is observed for LME-CP between 5,500 and 4,600 cal yr BP (Fig. 8). This timing coincides with ages between 4.5 and 5.7 ka determined for moraines in the vicinity of LME (Figs. 9 and 10, Fernández et al., 2012; Harrison et al., 2012; Nimick et al., 2016; Sagredo et al., 2018).

https://doi.org/10.5194/egusphere-2023-2156
Preprint. Discussion started: 25 September 2023

Predominance of terrigenous sediment supply is recorded at LME until 900 cal yr BP (end of Stage 3). Thus, erosion and fluvial transport of clastics dominated on Meseta Chile Chico. On the western slope of the North Patagonian Icefield, at Golfo Elefantes, sediment records document similar trends for grainsize variability between 4,800 and 850 cal yr BP (Fig. 10b), which are attributed to large precipitation-driven advances of the Gualas glacier (Bertrand et al., 2012). The correlation between both records suggests that more precipitation was responsible for higher influx of clastic and coarse (sandy) sediment to LME. We consider that the slight temporal offset between LME (5,500-900 cal yr BP) and Golfo Elefantes (4,800-850 cal yr BP) may be a consequence of asynchronous climate responses due to their relative positions with regard to the main Andean axis and the effect of calving processes that control west flowing glaciers at the North Patagonian Icefield (Harrison et al., 2012). However, such differences might as well be explained by dating uncertainties.

Humid conditions are documented by predominance of closed forests and low fire activity in the lower valley of Río Baker (Fig. 10e) and in Río Zeballos at ca. 5,800 and 5,300 cal yr, respectively (Iglesias et al., 2018; Mcculloch et al., 2017). The high sensibility of these sites and of the Meseta Chile Chico may be attributed to their high-altitude positions, and thus their enhanced exposure to the wet and/or cold conditions that triggered the expansion of glaciers of the Middle Holocene. Meanwhile, pollen reconstructions from other sites around the North Patagonian Icefield area do not indicate significant environmental changes around this time. In fact, they reveal discrepancies, with a decline in the Nothofagus forest accompanied by a higher magnitude and frequency of fire events between 3,800 and 2,000 cal yr BP (Maldonado et al., 2022). Further north, a similar trend is documented in the Río Cisnes Valley (Fig 1b), where the Nothofagus forest underwent retraction around 4,200 cal yr BP (De Porras et al., 2012; De Porras et al., 2014). This regional environmental signal for the Late Holocene period has been associated with marked seasonality, but it may also have been influenced by human occupation along these valleys during this time (De Porras et al., 2014; Maldonado et al., 2022). Nevertheless, whether strong climatic variability at are interannual-decadal scale played a major control in sedimentation on the Meseta Chile Chico eludes the scope of our sediment records.

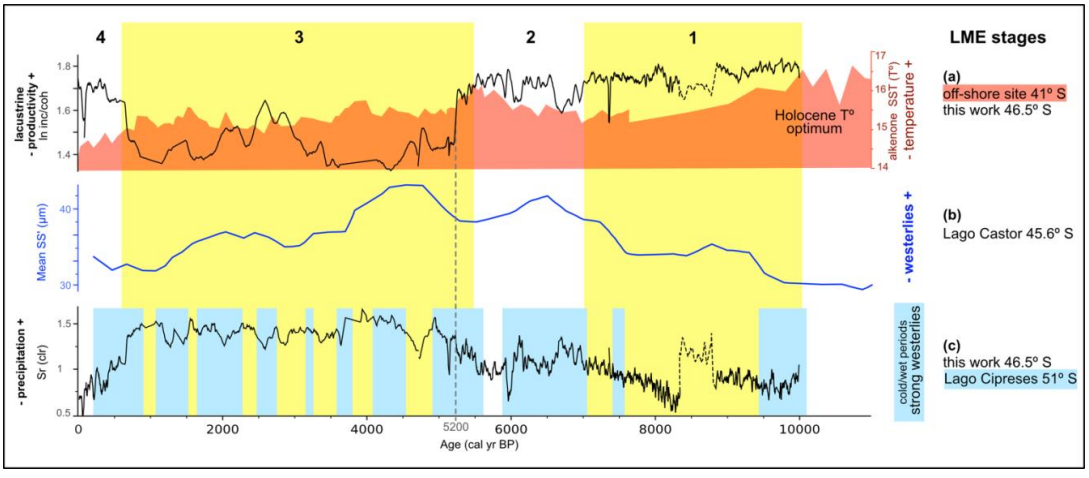

Figure 11: Proxies from LME in comparison to regional paleoclimate proxies. (a) Paleotemperatures according to an alkenone SST record (red) from marine sediments at 41º S (Lamy et al., 2002; Kilian and Lamy, 2012) and lacustrine productivity from LME (black). (c) Sr clr values (black) as proxy for fluvial runoff at Meseta Chile Chico and cold and wet period (light blue bands) based on the non-arboreal pollen record from Lago Cipreses (Moreno et al., 2018). (b) Mean of modified sortable silt values (10-125 µm: SS') of lake sediments from Lago Castor as proxy for bottom current and westerly wind intensities (Van Daele et al., 2016). Symbology is displayed in Figure 10.

https://doi.org/10.5194/egusphere-2023-2156
Preprint. Discussion started: 25 September 2023

Local studies on climate conditions do not constrain Holocene temperature variability and therefore we consider temperature reconstructions based on marine sediments, which are the only data available for Patagonia. Marine records from 41º S (Kaiser and Lamy, 2010; Lamy et al., 2007) and from South Patagonia at 53º S (Caniupan et al., 2011) show little correlation with our data (Fig. 11.a). However, the change from warmer to colder thermal conditions recorded by sea temperature is synchronous to the strong decrease of lacustrine productivity at ca. 5,300 cal yr BP, suggesting that temperature had a relevant control on the transition from Stage 2 to Stage 3 (Fig. 11a). Because ocean temperature reconstructions from the Pacific do not necessarily reflect thermal conditions of the eastern slope of the Andes, we consider that the influence of temperature at Meseta Chile Chico remains arguable. In contrast, our sedimentary records show a better correlation with different moisture proxies from our area throughout the Holocene (Fig. 10), pointing to precipitation as the main driver for this period rather than cooler temperatures.

To understand the relationship between our records and the SWW throughout the Holocene, we compared with proxies from nearby sites, including sites located east of the main Andean axis. Studies based on modern climate records indicate that leeward (east) of the Andes stronger westerlies induce lower moisture and higher evaporation and, therefore, are associated with dry periods (Garreaud et al., 2013) and lake level changes (Kilian and Lamy, 2012). The opposite trend is documented west of the Andes, where the relationship between wet conditions and westerly wind activities is direct.

We observe that the correlation between Lago Castor estimations of the SWW (Van Daele et al., 2016) and our records is not straight forward (Fig. 11b). Nonetheless, maximum wind intensities from this site and highest precipitation conditions around the Middle Holocene in our studied area are synchronous. Meanwhile, SWW reconstructions from Lago Cipreses (Fig. 11c, Moreno et al., 2018) suggest a predominance of strong westerlies phases with intensified precipitation between 7,000 and 5,900 (Stage 2), and between 5,500 and 900 cal yr BP (Stage 3) in the Meseta Chile Chico.

In consequence, high precipitation periods in our study area seem to have been mainly driven by high SWW activity associated to their northward expansion (Lamy et al., 2010), bringing cold/wet phases into the middle latitudes, which started around 7,000-8,500 cal yr BP, but became predominant around 5,000 cal yr BP. The frequency of these intervals was mainly controlled by changes on a millennial to centennial scale of the Southern Annular Mode (SAM, Moreno et al., 2018). Therefore, our findings imply that the SAM-driven climatic conditions that triggered neoglaciations in Antarctica and Southern Patagonia (Kaplan et al., 2020), extended as well into Central West Patagonia.

Additionally, the straightforward relation between precipitation at Meseta Chile Chico and the SWW indicate that the eastern slope of the Andean range was a transition zone between the humid Andes and the dry steppe region, over which this wind belt still retained moisture from the Pacific Ocean during the Early-Middle Holocene.

After 1,000 cal yr BP, LME sediments document a shift back to higher accumulation of biogenic components with less clastic input. This tendency continues until 300 cal yr BP. Predominance of silt and clay for our record (Unit A) refers either to a moderate erosion intensity uncapable of transporting sand but enough to cause watershed erosion, and/or to enhanced influx of clay-silt sized minerogenic clasts, such as micaceous minerals, caused by higher chemical weathering of rocks that occupy the catchment of LME.

Between 300 and 200 cal yr BP, inc/coh ratio reaches high values and, in consequence, a strong drop is observed in elemental data (Ca/Ti, Ti and Sr) as well as in sand percentages (Fig. 8). The age of this signal overlaps with the Late Holocene glacial period also known as “Little Ice age” (Davies et al., 2020) and widely documented within our study area (Davies and Glasser, 2012; Garibotti and Villalba, 2017; Nimick et al., 2016; Sagredo et al., 2021). However, a high lacustrine productivity signal suggests that favourable and more temperate rather than cold/wet conditions controlled the environment at Meseta Chile Chico. This points to a climate signal being overprinted by local sedimentation dynamics at Meseta Chile Chico, and that low allochthonous input was mainly responsible for high lake production at LME at this time. However, the unclear signal of our record could also be the result of the resolution of our age-depth model for the Late Holocene (2000-0 cal yr BP). We expect

https://doi.org/10.5194/egusphere-2023-2156
Preprint. Discussion started: 25 September 2023

to address these paleoenvironmental issues with more detail for this period with further investigations from other records of the Meseta Chile Chico area.

Although human presence east of the North Patagonian Icefield became regular at 3,000 cal yr BP, dated archaeological sites along the SE border of Meseta Chile Chico point to human occupancy between 500 and 1,560 cal yr BP (Nuevo-Delaunay et al., 2022). However, preliminary archaeological surveys across the plateau revealed small surface concentrations of lithic material indicating the procurement of toolstones, signalling a minimal evidence of anthropogenic influence on Meseta Chile Chico during the Holocene (Méndez et al. 2023). Therefore, we assume that also the younger section of LME-CP (Stage 4) reflects mainly natural Holocene environmental variability.

6.2 Sedimentary environments at the Meseta Chile Chico throughout the Holocene

According to glacial reconstructions within our study area, the glaciers of the Parque Nacional Patagonia icefield that covered the Meseta Chile Chico during the LGM had already begun their retreat before 10 ka (subchapter 6.1). They also indicate that glaciers at other sites from West Patagonia mostly continued retreating until ca. 6 ka and that they presented several advance/retreat cycles between 6 and 0.2 ka (Davies et al., 2020; Benito et al., 2021; Glasser et al., 2005). Therefore, we consider the possibility that the westernmost glaciers of the Parque Nacional Patagonia icefield advanced and retreated several times from the Meseta Chile Chico before permanently abandoning this catchment system in the Holocene. Moreover, the extension of the basin and catchment of LME and the Chile Chico Meseta drainage system must have been largely affected by geomorphological responses to glacial dynamics during this time.

Maximum lake productivity (inc/coh ratio) recorded at the lowermost layers of LME sediments (Stage 1), suggest that its oldest sediments were accumulated when LME was already a distal lake basin with respect to the glaciers of the Parque Nacional Patagonia Icefield. Furthermore, the fine grainsize of the minerogenic components (high silt/sand ratios) and the lamination (units C, D, E, G and H, Fig. 3) of Stages 1 and 2 are characteristic of fluvioglacial settings. In these settings silt-sized sediment is transported by downwashing and reworking of freshly exposed glacier deposits and accumulated downslope by particle settling in the nearby lake basins (Ballantyne, 2003).

Glacial conditions on Meseta Chile Chico that might have persisted until the Middle Holocene agree with the abrupt switch from autochthonous to allochthonous sedimentation recorded at the beginning of Stage 3. If we assume a distal glacial source for Stages 1 and 2, then it is also possible that the Middle Holocene glacier advance recorded in the moraines around our study area, might have triggered an eastward advance of the outlet glaciers of the Parque Nacional Patagonia icefield into Meseta Chile Chico and, therefore, enlarging its catchment area. Former studies on glaciolacustrine sediments associate the occurrence of laminated sandy layers with historically recorded glacial stages (Leemann and Niessen, 1994), indicating that such an advance could be the source of sand clasts and additional detrital signals in the sediments of Stage 3. The occurrence of a Middle Holocene glacial advance in our studied plateau is also supported by regional proxies, which indicate lower temperatures and a higher precipitation regime for Central Patagonia during this period (Figs. 10 and 11, Bertrand et al., 2012; de Porras et al., 2012; Iglesias et al., 2018; Kilian and Lamy, 2012).

As geomorphological mapping shows (Davies et al., 2020; this work), even after the Patagonian Park Range Icefield had retreated from the Meseta Chile Chico, smaller glaciers remained around the summit of Cerro Pico Sur for a longer period (Fig. 1c). These glaciers might be responsible for second order oscillations within our data during Stage 3, since restricted glacial advances are documented around the North Patagonian Icefield between ca. 4.3-1.2 ka at Lago Colonia, Lago León, Cerro San Lorenzo and Golfo Elefantes (Bertrand et al., 2012; Harrison et al., 2008; Nimick et al., 2016; Sagredo et al., 2021) as well as at other sites from South Patagonia (Hall et al., 2019; Reynhout et al., 2019; Strelin et al., 2014).

It is not possible to estimate when glacial influence ceased on Meseta Chile Chico during the Holocene. This event would have triggered the transition of LME from a fluvioglacial basin into a fluvial basin. Nonetheless, the steady increase in sand/silt

https://doi.org/10.5194/egusphere-2023-2156
Preprint. Discussion started: 25 September 2023

ratios between ca 2,500 and 900 cal yr BP might be indicative of the settling of a mature fluvial system after paraglacial reworking had ended on this plateau.

It is likely that also aeolian transport variably contributed to sediment accumulation in LME. Sedimentation of fine sediment originating from deflation of recently exposed glacial deposits after ice recession, is a characteristic process within paraglacial environments (Ballantyne, 2003). Accordingly, high silt/sand ratios of Stages 1 and 2 could have a secondary eolian component. In contrast, sediment layers for Stage 3 are sand dominated. Because sand can only be wind-transported by saltation, wind driven accumulation of sediments in Stage 3 would have required a proximal constant source of sand sized detrital material. We consider it as unlikely that such a source could have developed in an isolated high-altitude area, dominated by volcanic rocks such the Meseta Chile Chico. Moreover, small fluctuations of sand percentages in LME within Stage 3 do not correlate with SWW intensity records from Patagonia. Therefore, within our studied area, wind sedimentation was probably overprinted by glaciofluvial and/or fluvial processes strongly linked to the rapidly changing wet/dry conditions that controlled landscape evolution in Patagonia after deglaciation during the Holocene.

At the end of Stage 3 (900 cal yr BP), LME changed back to high lake productivity and high silt/sand ratio conditions, which remained relatively stable until modern times (Stage 4). This suggests that around this period the sedimentary environment of Meseta Chile Chico evolved into the low gradient and ephemeral streams that currently control sediment supply at LME and its nearby lakes. Since regional proxies and recors from this work are non-conclusive for precipitation/temperature variability around this time (Fig 10), we attribute this episode to local changes such as catchment morphology, weathering and slope gradients.

Sediment changes within our records are consistent with two scenarios: i) a fluvial basin, controlled mainly by precipitation driven changes in superficial runoff; ii) a glacial or periglacial setting, controlled by episodes of glacier advance and retreat that were induced by both thermal (at least until the Middle Holocene) and precipitation oscillations, until a fluvial system was established sometime after 5,500 cal yr BP. Nonetheless, it is most likely that these environments coexisted and also alternated throughout the Holocene period in the Meseta Chile Chico. Additionally, ice reconstructions for plateau icefields are challenging since evidence of glaciation is commonly scarce. In these settings, glacier dynamics are directly dependent on plateau area, main wind direction and altitude (Rea et al., 1998; Rea and Evans, 2003), thus they can be asynchronous to valley glaciers. Therefore, due to the lack of moraine chronologies for Meseta Chile Chico, the existence of glacial advances after the LGM remains speculative.

7 Conclusions

The sediment record of LME started before ~10,000 cal yr BP, when ice of the LGM retreated from Meseta Chile Chico. With the exception of two isolated wetter periods (7,000-6,500 and 6,200-5,900 cal yr BP), glacier recession caused by temperate and drier conditions continued between 10,000-6,000 cal yr BP, delivering low amounts of minerogenic components into the lake. Environmental conditions for accumulation of biogenic lacustrine sediments were optimal during this period but a steadily decrease. Around 8,300 cal yr BP, fall-out deposits originating from the H1 eruption of Hudson volcano reached the lake with deposition of primary and remobilized tephra.

At 5,500 cal yr BP, there was a notable shift in sedimentation in the Meseta Chile Chico region from organic to allochthonous minerogenic material. This shift was primarily driven by increased fluvial erosion of basaltic rocks, which, in turn, were influenced by higher precipitation associated with stronger SWW activity and glacial advances in Patagonia.

Between 900 and 300 cal yr BP terrigenous input decreased again. At 300 cal yr BP sediment accumulation stabilized and was mainly controlled by lacustrine productivity without major changes until modern times. This indicates that the present day Meseta Chile Chico sedimentation reflects similar environmental conditions as in the past 300 years.

https://doi.org/10.5194/egusphere-2023-2156
Preprint. Discussion started: 25 September 2023

Changes in granulometry and provenance of the sediments of LME are consistent with glacial advances and retreats in the catchment until the Late Holocene. However, since there are no moraine dates available for Meseta Chile Chico, it is not clear when glaciers definitively retreated from this area.

The lithological variability recorded by the lacustrine sediment record from Meseta Chile Chico, its altitude and proximity to the North Patagonian Icefield as well as the low degree of human influences provides a privileged setting for a detailed study of Holocene environmental conditions.

Data availability

Original contributions presented in this study are included in materials supplementary to this article and available online at https://doi.pangaea.de/10.1594/PANGAEA.961940

Author contribution

The objectives of this study as well as the planning for sampling campaigns was carried out by C. Franco, A. Maldonado, M.E. de Porras, A. Nuevo-Delaunay, and C. Méndez. Analytical lab work was carried out by C. Franco, A Maldonado, C. Ohlendorf, and A.C. Gebhardt. Lithological descriptions, age-depth model, and tephrochronology, as well as manuscript writing was performed by C. Franco. B. Zolitschka and A. Maldonado conceptualized this research. All authors contributed to writing and revising this manuscript.

Competing interest

The authors declare that they have no conflict of interest.

Acknowledgements

Thanks go to Rafael Stiens, Pascal Daub and Claudia Hernandez and the University of Oldenburg for supporting analytical work. To Stella Birlo for her assistance with python coding. To Corporación Nacional Forestal (CONAF, Chile) for authorising our studies in wild protected areas of the Meseta Chile Chico.

Funding

This study is supported by the German Academic Exchange Service (DAAD, Research Grants – Doctoral Programmes in Germany), and ANID FONDECYT 1210042 and ANID Regional R20F0002 grants (Ministry of Science, Chile).

References

Aniya, M.: Holocene Glacial Chronology in Patagonia: Tyndall and Upsala Glaciers, Arct. Alp. Res., 27, 311-322, 10.2307/1552024, 1995.

Ballantyne, C. K.: Paraglacial Landsystems, in: Glacial Landsystems, edited by: Evans, D. J. A., Arnold, 2003.

Bas, M. J. L., Maitre, R. W. L., Streckeisen, A., Zanettin, B., and Rocks, I. S. o. t. S. o. I.: A Chemical Classification of Volcanic Rocks Based on the Total Alkali-Silica Diagram, J. Petrol., 27, 745-750, 10.1093/petrology/27.3.745, 1986.

Bendle, J. M., Thorndycraft, V. R., and Palmer, A. P.: The glacial geomorphology of the Lago Buenos Aires and Lago Pueyrredón ice lobes of central Patagonia, J. Maps, 13, 654-673, 10.1080/17445647.2017.1351908, 2017a.

https://doi.org/10.5194/egusphere-2023-2156
Preprint. Discussion started: 25 September 2023

Bendle, J. M., Palmer, A. P., Thorndycraft, V. R., and Matthews, I. P.: High-resolution chronology for deglaciation of the Patagonian Ice Sheet at Lago Buenos Aires (46.5°S) revealed through varve chronology and Bayesian age modelling, Quat. Sci. Rev., 177, 314-339, https://doi.org/10.1016/j.quascirev.2017.10.013, 2017b.

Benito, G. and Thorndycraft, V. R.: Catastrophic glacial-lake outburst flooding of the Patagonian Ice Sheet, Earth Sci. Rev., 200, 102996, https://doi.org/10.1016/j.earscirev.2019.102996, 2020.

Benito, G., Thorndycraft, V. R., Medialdea, A., Machado, M. J., Sancho, C., and Dussaillant, A.: Declining discharge of glacier outburst floods through the Holocene in central Patagonia, Quat. Sci. Rev., 256, 106810, https://doi.org/10.1016/j.quascirev.2021.106810, 2021.

Bertrand, S., Hughen, K. A., Lamy, F., Stuut, J. B. W., Torrejón, F., and Lange, C. B.: Precipitation as the main driver of Neoglacial fluctuations of Gualas glacier, Northern Patagonian Icefield, Clim. Past, 8, 519-534, 10.5194/cp-8-519-2012, 2012.

Blaauw, M. and Christen, J.: Flexible Paleoclimate Age-Depth Models Using an Autoregressive Gamma Process, Bayesian Analysis, 6, 457-474, 10.1214/11-BA618, 2011.

Boex, J., Fogwill, C., Harrison, S., Glasser, N. F., Hein, A., Schnabel, C., and Xu, S.: Rapid thinning of the Late Pleistocene Patagonian Ice Sheet followed migration of the Southern Westerlies, Sci Rep, 3, 2118, 10.1038/srep02118, 2013.

Boygle, J.: Variability of tephra in lake and catchment sediments, Svínavatn, Iceland, Global Planet. Change, 21, 129-149, https://doi.org/10.1016/S0921-8181(99)00011-9, 1999.

Burnett, A. P., Soreghan, M. J., Scholz, C. A., and Brown, E. T.: Tropical East African climate change and its relation to global climate: A record from Lake Tanganyika, Tropical East Africa, over the past 90+kyr, Palaeogeogr. Palaeoclimatol. Palaeoecol., 303, 155-167, https://doi.org/10.1016/j.palaeo.2010.02.011, 2011.

Caldenius, C. C. Z.: Las Glaciaciones Cuaternarias en la Patagonia y Tierra del Fuego, Geogr. Ann., 14, 1-164, 10.1080/20014422.1932.11880545, 1932.

Caniupan, M., Lamy, F., Lange, C., Kaiser, J., Arz, H., Kilian, R., Baeza, O., Aracena, C., Hebbeln, D., Kissel, C., Laj, C., and Mollenhauer, G.: Millennial-scale sea surface temperature and Patagonian Ice Sheet changes off southernmost Chile (53°S) over the past ~60 kyr, Paleoceanography, 26, PA3221, 10.1029/2010PA002049, 2011.

Clapperton, C. M. and Sugden, D. E.: Holocene glacier fluctuations in South America and Antarctica, Quat. Sci. Rev., 7, 185-198, https://doi.org/10.1016/0277-3791(88)90005-4, 1988.

Croudace, I., Rindby, A., and Rothwell, R.: ITRAX: Description and Evaluation of a New Multi-Function X-ray Core Scanner, Geological Society, London, Special Publications, 267, 51-63, 10.1144/GSL.SP.2006.267.01.04, 2006.

Davies, B. J. and Glasser, N. F.: Accelerating shrinkage of Patagonian glaciers from the Little Ice Age (~AD 1870) to 2011, J. Glaciol., 58, 1063-1084, 10.3189/2012JoG12J026, 2012.

Davies, B. J., Thorndycraft, V. R., Fabel, D., and Martin, J. R. V.: Asynchronous glacier dynamics during the Antarctic Cold Reversal in central Patagonia, Quat. Sci. Rev., 200, 287-312, https://doi.org/10.1016/j.quascirev.2018.09.025, 2018.

Davies, B. J., Darvill, C. M., Lovell, H., Bendle, J. M., Dowdeswell, J. A., Fabel, D., García, J. L., Geiger, A., Glasser, N. F., Gheorghiu, D. M., Harrison, S., Hein, A. S., Kaplan, M. R., Martin, J. R. V., Mendelova, M., Palmer, A., Pelto, M., Rodés, Á., Sagredo, E. A., Smedley, R. K., Smellie, J. L., and Thorndycraft, V. R.: The evolution of the Patagonian Ice Sheet from 35 ka to the present day (PATICE), Earth Sci. Rev., 204, 103152, https://doi.org/10.1016/j.earscirev.2020.103152, 2020.

Davies, S., Lamb, H., and Roberts, S.: Micro-XRF Core Scanning in Palaeolimnology: Recent Developments, in, 189-226, 10.1007/978-94-017-9849-5_7, 2015.

De la Cruz, R. and Suárez, M.: Geology of the area Chile Chico-Río de las Nieves, Carlos Ibáñez del Campo Region, Servicio Nacional de Geología y Minería, 116, 2008.

de Porras, M. E., Maldonado, A., Quintana, F. A., Martel-Cea, A., Reyes, O., and Méndez, C.: Environmental and climatic changes in central Chilean Patagonia since the Late Glacial (Mallín El Embudo, 44° S), Clim. Past, 10, 1063-1078, 10.5194/cp-10-1063-2014, 2014.

https://doi.org/10.5194/egusphere-2023-2156
Preprint. Discussion started: 25 September 2023

de Porras, M. E., Maldonado, A., Abarzúa, A. M., Cárdenas, M. L., Francois, J. P., Martel-Cea, A., Stern, C. R., Méndez, C., and Reyes, O.: Postglacial vegetation, fire and climate dynamics at Central Chilean Patagonia (Lake Shaman, 44°S), Quat. Sci. Rev., 50, 71-85, https://doi.org/10.1016/j.quascirev.2012.06.015, 2012.

Douglass, D., Singer, B., Kaplan, M., Ackert, R., Mickelson, D., and Caffee, M.: Evidence of early Holocene glacial advances in southern South America from cosmogenic surface-exposure dating, Geology, 33, 237-240, 10.1130/G21144.1, 2005a.

Douglass, D. C., Singer, B. S., Kaplan, M. R., Mickelson, D. M., and Caffee, M.: Cosmogenic Surface-Exposure Dating of Boulders on Last-Glacial and Late-Glacial Moraines, Lago Buenos Aires, Argentina: Interpretive Strategies and Paleoclimate Implications, Quaternary Geochronology, 2005, 43-58, 2005b.

Espinoza, F., Morata, D., Pelleter, E., Maury, R., Guivel, C., Suárez, M., Lagabrielle, Y., Polve, M., Bellon, H., Cotten, J., and R, D.: Petrogenesis of the Eocene and Mio-Pliocene alkaline basaltic magmatism in Meseta Chile chico, southern Patagonia, Chile : evidence of two slab window processes, Lithos, 3-4, 314-343, 2005.

Fernandez, R., Anderson, J., Bertrand, S., and Wellner, J.: Gualas Glacier sedimentary record of climate and environmental change, Golfo Elefantes, Western Patagonia (46.5°S), The Holocene, 22, 451-463, 10.1177/0959683611425545, 2012.

Futa, K. and Stern, C. R.: Sr and Nd isotopic and trace element compositions of Quaternary volcanic centers of the Southern Andes, Earth Planet. Sci. Lett., 88, 253-262, https://doi.org/10.1016/0012-821X(88)90082-9, 1988.

García, J. L., Maldonado, A., de Porras, M. E., Nuevo Delaunay, A., Reyes, O., Ebensperger, C. A., Binnie, S. A., Lüthgens, C., and Méndez, C.: Early deglaciation and paleolake history of Río Cisnes Glacier, Patagonian Ice Sheet (44°S), Quat. Res., 91, 194-217, 10.1017/qua.2018.93, 2019.

Garibotti, I. A. and Villalba, R.: Lichenometric dating using Rhizocarpon subgenus Rhizocarpon in the Patagonian Andes, Argentina, Quat. Res., 71, 271-283, https://doi.org/10.1016/j.yqres.2009.01.012, 2009.

Garreaud, R., Lopez, P., Minvielle, M., and Rojas, M.: Large-Scale Control on the Patagonian Climate, J. Clim., 26, 215-230, 10.1175/JCLI-D-12-00001.1, 2013.

Glasser, N. F. and Jansson, K. N.: Fast-flowing outlet glaciers of the Last Glacial Maximum Patagonian Icefield, Quat. Res., 63, 206-211, 10.1016/j.yqres.2004.11.002, 2005.

Glasser, N. F., Harrison, S., and Jansson, K. N.: Topographic controls on glacier sediment–landform associations around the temperate North Patagonian Icefield, Quat. Sci. Rev., 28, 2817-2832, https://doi.org/10.1016/j.quascirev.2009.07.011, 2009.

Glasser, N. F., Harrison, S., Winchester, V., and Aniya, M.: Late Pleistocene and Holocene palaeoclimate and glacier fluctuations in Patagonia, Global Planet. Change, 43, 79-101, https://doi.org/10.1016/j.gloplacha.2004.03.002, 2004.

Glasser, N. F., Jansson, K. N., Harrison, S., and Rivera, A.: Geomorphological evidence for variations of the North Patagonian Icefield during the Holocene, Geomorphology, 71, 263-277, https://doi.org/10.1016/j.geomorph.2005.02.003, 2005.

Glasser, N. F., Jansson, K. N., Duller, G. A. T., Singarayer, J., Holloway, M., and Harrison, S.: Glacial lake drainage in Patagonia (13-8 kyr) and response of the adjacent Pacific Ocean, Sci. Rep., 6, 21064, 10.1038/srep21064, 2016.

Grove, J. M.: in: The Little Ice Ages: Ancient and Modern 2nd ed., Routledge, Oxfordshire, England, UK, 405-504, https://doi.org/10.4324/9780203505205, 2004.

Guyard, H., Chapron, E., St-Onge, G., Anselmetti, F. S., Arnaud, F., Magand, O., Francus, P., and Mélières, M.-A.: High-altitude varve records of abrupt environmental changes and mining activity over the last 4000 years in the Western French Alps (Lake Bramant, Grandes Rousses Massif), Quat. Sci. Rev., 26, 2644-2660, https://doi.org/10.1016/j.quascirev.2007.07.007, 2007.

Hall, B. L., Lowell, T. V., Bromley, G. R. M., Denton, G. H., and Putnam, A. E.: Holocene glacier fluctuations on the northern flank of Cordillera Darwin, southernmost South America, Quat. Sci. Rev., 222, 105904, https://doi.org/10.1016/j.quascirev.2019.105904, 2019.

Harrison, S., Glasser, N. F., Duller, G. A. T., and Jansson, K. N.: Early and mid-Holocene age for the Tempanos moraines, Laguna San Rafael, Patagonian Chile, Quat. Sci. Rev., 31, 82-92, https://doi.org/10.1016/j.quascirev.2011.10.015, 2012.

https://doi.org/10.5194/egusphere-2023-2156
Preprint. Discussion started: 25 September 2023

Harrison, S., Glasser, N., Winchester, V., Haresign, E., Warren, C., Duller, G. A. T., Bailey, R., Ivy-Ochs, S., Jansson, K., and Kubik, P.: Glaciar León, Chilean Patagonia: late-Holocene chronology and geomorphology, The Holocene, 18, 643-652, 10.1177/0959683607086771, 2008.

Hein, A. S., Hulton, N. R. J., Dunai, T. J., Sugden, D. E., Kaplan, M. R., and Xu, S.: The chronology of the Last Glacial Maximum and deglacial events in central Argentine Patagonia, Quat. Sci. Rev., 29, 1212-1227, https://doi.org/10.1016/j.quascirev.2010.01.020, 2010.

Henríquez, W. I., Villa-Martínez, R., Vilanova, I., De Pol-Holz, R., and Moreno, P. I.: The last glacial termination on the eastern flank of the central Patagonian Andes (47 ° S), Clim. Past, 13, 879-895, 10.5194/cp-13-879-2017, 2017.

Hogg, A. G., Heaton, T. J., Hua, Q., Palmer, J. G., Turney, C. S. M., Southon, J., Bayliss, A., Blackwell, P. G., Boswijk, G., Bronk Ramsey, C., Pearson, C., Petchey, F., Reimer, P., Reimer, R., and Wacker, L.: SHCal20 Southern Hemisphere Calibration, 0–55,000 Years cal BP, Radiocarbon, 62, 759-778, 10.1017/RDC.2020.59, 2020.

Hulton, N., Sugden, D., Payne, A., and Clapperton, C.: Glacier Modeling and the Climate of Patagonia during the Last Glacial Maximum, Quat. Res., 42, 1-19, https://doi.org/10.1006/qres.1994.1049, 1994.

Iglesias, V., Haberle, S. G., Holz, A., and Whitlock, C.: Holocene Dynamics of Temperate Rainforests in West-Central Patagonia, Frontiers in Ecology and Evolution, 5, 177, 10.3389/fevo.2017.00177, 2018.

Kaiser, J. and Lamy, F.: Links between Patagonian Ice Sheet fluctuations and Antarctic dust variability during the last glacial period (MIS 4-2), Quat. Sci. Rev., 29, 1464-1471, 10.1016/j.quascirev.2010.03.005, 2010.

Kaplan, M. R., Strelin, J. A., Schaefer, J. M., Peltier, C., Martini, M. A., Flores, E., Winckler, G., and Schwartz, R.: Holocene glacier behavior around the northern Antarctic Peninsula and possible causes, Earth Planet. Sci. Lett., 534, 116077, https://doi.org/10.1016/j.epsl.2020.116077, 2020.

Kaplan, M. R., Schaefer, J. M., Strelin, J. A., Denton, G. H., Anderson, R. F., Vandergoes, M. J., Finkel, R. C., Schwartz, R., Travis, S. G., Garcia, J. L., Martini, M. A., and Nielsen, S. H. H.: Patagonian and southern South Atlantic view of Holocene climate, Quat. Sci. Rev., 141, 112-125, https://doi.org/10.1016/j.quascirev.2016.03.014, 2016.

Kilian, R. and Lamy, F.: A review of Glacial and Holocene paleoclimate records from southernmost Patagonia (49–55°S), Quat. Sci. Rev., 53, 1-23, https://doi.org/10.1016/j.quascirev.2012.07.017, 2012.

Lamy, F., Rühlemann, C., Hebbeln, D., and Wefer, G.: High- and low-latitude climate control on the position of the southern Peru-Chile Current during the Holocene, Paleoceanography, 17, 10.1029/2001PA000727, 2002.

Lamy, F., Kilian, R., Arz, H. W., Francois, J.-P., Kaiser, J., Prange, M., and Steinke, T.: Holocene changes in the position and intensity of the southern westerly wind belt, Nat. Geosci., 3, 695-699, 10.1038/ngeo959, 2010.

Lamy, F., Kaiser, J., Arz, H. W., Hebbeln, D., Ninnemann, U., Timm, O., Timmermann, A., and Toggweiler, J. R.: Modulation of the bipolar seesaw in the Southeast Pacific during Termination 1, Earth Planet. Sci. Lett., 259, 400-413, https://doi.org/10.1016/j.epsl.2007.04.040, 2007.

Leemann, A. and Niessen, F.: Holocene glacial activity and climatic variations in the Swiss Alps: reconstructing a continuous record from proglacial lake sediments, The Holocene, 4, 259-268, 10.1177/095968369400400305, 1994.

Lopez-Escobar, L., Kilian, R., Kempton, P. D., and Tagiri, M.: Petrography and geochemistry of Quaternary rocks from the Southern Volcanic Zone of the Andes between 41°30′ and 46°00′S, Chile, Rev. Geol. Chile, 20, 33-55, 1993.

Maldonado, A., De Porras, M., Martel-Cea, A., Reyes, O., Nuevo-Delaunay, A., and Méndez, C.: Holocene Environmental Dynamics of the Lago Cochrane/Pueyrredón Valley, Central West Patagonia (47°S), Front. Earth Sci., 10, 833637, 10.3389/feart.2022.833637, 2022.

McCulloch, R. D., Figuerero Torres, M. J., Mengoni Goñalons, G. L., Barclay, R., and Mansilla, C.: A Holocene record of environmental change from Río Zeballos, central Patagonia, The Holocene, 27, 941-950, 10.1177/0959683616678460, 2017.

Melles, M., Brigham-Grette, J., Minyuk, P. S., Nowaczyk, N. R., Wennrich, V., DeConto, R. M., Anderson, P. M., Andreev, A. A., Coletti, A., Cook, T. L., Haltia-Hovi, E., Kukkonen, M., Lozhkin, A. V., Rosén, P., Tarasov, P., Vogel, H., and Wagner,

https://doi.org/10.5194/egusphere-2023-2156
Preprint. Discussion started: 25 September 2023

B.: 2.8 Million Years of Arctic Climate Change from Lake Elgygytgyn, NE Russia, Science, 337, 315-320, doi:10.1126/science.1222135, 2012.

Méndez, C., Nuevo-Delaunay, A., and Reyes, O.: The exploration of marginal spaces in Central-West Patagonia and the role of discontinuous occupation of forests and highlands, L'Anthropologie, 127, 103118, https://doi.org/10.1016/j.anthro.2023.103118, 2023.

Mercer, J. H.: Glacial history of southernmost South America, Quat. Res., 6, 125-166, https://doi.org/10.1016/0033-5894(76)90047-8, 1976.

Moreno, P. I., Vilanova, I., Villa-Martínez, R., Dunbar, R. B., Mucciarone, D. A., Kaplan, M. R., Garreaud, R. D., Rojas, M., Moy, C. M., De Pol-Holz, R., and Lambert, F.: Onset and Evolution of Southern Annular Mode-Like Changes at Centennial Timescale, Sci. Rep., 8, 3458, 10.1038/s41598-018-21836-6, 2018.

Müller, P. J. and Schneider, R.: An automated leaching method for the determination of opal in sediments and particulate matter, Deep Sea Res. Part I, 40, 425-444, https://doi.org/10.1016/0967-0637(93)90140-X, 1993.

Naranjo, J. A. and Stern, C. R.: Holocene explosive activity of Hudson Volcano, southern Andes, Bull. Volcanol., 59, 291-306, 10.1007/s004450050193, 1998.

Naranjo, J. A. and Stern, C. R.: Holocene tephrochronology of the southernmost part (42°30'-45°S) of the Andean Southern Volcanic Zone, Rev. Geol. Chile, 31, 224-240, 2004.

Nimick, D. A., McGrath, D., Mahan, S. A., Friesen, B. A., and Leidich, J.: Latest Pleistocene and Holocene glacial events in the Colonia valley, Northern Patagonia Icefield, southern Chile, J. Quat. Sci., 31, 551-564, 10.1002/jqs.2847, 2016.

Nuevo-Delaunay, A., Méndez, C., Reyes, O., Seelenfreund, A., and Belmar, C.: La ocupación humana antigua de los callejones sin salida de los Andes de Patagonia: Midiendo la intensidad de uso del espacio en los márgenes del Campo de Hielo Norte (Aisén, Chile), Chungara Revista de Antropología Chilena, 54, 481-500, 10.4067/S0717-73562022005000203, 2022.

Porter, S. C.: Onset of neoglaciation in the southern hemisphere, J. Quat. Sci., 15, 395-408, 10.1002/1099-1417(200005)15:4<395::AID-JQS535>3.0.CO;2-H, 2000.

Rabassa, J., Coronato, A. M., and Salemme, M.: Chronology of the Late Cenozoic Patagonian glaciations and their correlation with biostratigraphic units of the Pampean region (Argentina), J. S. Am. Earth. Sci., 20, 81-103, https://doi.org/10.1016/j.jsames.2005.07.004, 2005.

Rea, B., Whalley, B., Evans, D., Gordon, J., and McDougall, D.: Plateau Icefields: Geomorphology and dynamics, J. Quat. Sci., 13, 35-54, 1998.

Rea, B. R. and Evans, D. J. A.: Plateau Icefield Landsystems, in: Glacial Landsystems, edited by: Evans, D. J. A., Arnold, 2003.

Reynhout, S. A., Kaplan, M. R., Sagredo, E. A., Aravena, J. C., Soteres, R. L., Schwartz, R., and Schaefer, J. M.: Holocene glacier history of northeastern Cordillera Darwin, southernmost South America (55°S), Quat. Res., 105, 166-881, 10.1017/qua.2021.45, 2021.

Reynhout, S. A., Sagredo, E. A., Kaplan, M. R., Aravena, J. C., Martini, M. A., Moreno, P. I., Rojas, M., Schwartz, R., and Schaefer, J. M.: Holocene glacier fluctuations in Patagonia are modulated by summer insolation intensity and paced by Southern Annular Mode-like variability, Quat. Sci. Rev., 220, 178-187, https://doi.org/10.1016/j.quascirev.2019.05.029, 2019.

Sagredo, E., Reynhout, S., Kaplan, M., Aravena, J., Araya, P., Luckman, B., Schwartz, R., and Schaefer, J.: Holocene History of Río Tranquilo Glacier, Monte San Lorenzo (47°S), Central Patagonia, Front. Earth Sci., 9, 813433, 10.3389/feart.2021.813433, 2021.

Sagredo, E. A., Kaplan, M. R., Araya, P. S., Lowell, T. V., Aravena, J. C., Moreno, P. I., Kelly, M. A., and Schaefer, J. M.: Trans-pacific glacial response to the Antarctic Cold Reversal in the southern mid-latitudes, Quat. Sci. Rev., 188, 160-166, https://doi.org/10.1016/j.quascirev.2018.01.011, 2018.

https://doi.org/10.5194/egusphere-2023-2156
Preprint. Discussion started: 25 September 2023

Singer, B. S., Ackert, R. P., Jr., and Guillou, H.: 40Ar/39Ar and K-Ar chronology of Pleistocene glaciations in Patagonia, GSA Bulletin, 116, 434-450, 10.1130/b25177.1, 2004.

Smedley, R. K., Glasser, N. F., and Duller, G. A. T.: Luminescence dating of glacial advances at Lago Buenos Aires (~46 °S), Patagonia, Quat. Sci. Rev., 134, 59-73, https://doi.org/10.1016/j.quascirev.2015.12.010, 2016.

Stern, C., Henríquez, W., Villa-Martínez, R., Sagredo, E., Aravena, J., and De Pol-Holz, R.: Holocene tephrochronology around Cochrane (~47° S), southern Chile, Andean Geol., 43, 1-19, 10.5027/andgeoV43n1-a01, 2016.

Stern, C. R.: Mid-Holocene tephra on Tierra del Fuego (54°S) derived from the Hudson volcano (46°S): evidence for a large explosive eruption., Rev. Geol. Chile, 18, 139-146, 1991.

Stern, C. R.: Holocene tephrochronology record of large explosive eruptions in the southernmost Patagonian Andes, Bull. Volcanol., 70, 435-454, 10.1007/s00445-007-0148-z, 2008.

Stosch, H.-G.: TAS diagram, K2O-SiO2 diagram and AFM diagram template for Excel (1.1), Zenodo. https://doi.org/10.5281/zenodo.7086317, 2022.

Strelin, J. A., Kaplan, M. R., Vandergoes, M. J., Denton, G. H., and Schaefer, J. M.: Holocene glacier history of the Lago Argentino basin, Southern Patagonian Icefield, Quat. Sci. Rev., 101, 124-145, https://doi.org/10.1016/j.quascirev.2014.06.026, 2014.

Sugden, D. E., Bentley, M. J., Fogwill, C. J., Hulton, N. R. J., McCulloch, R. D., and Purves, R. S.: Late-Glacial Glacier Events in Southernmost South America: A Blend of 'Northern' and 'Southern' Hemispheric Climatic Signals?, Geogr. Ann. Ser. A Phys. Geogr., 87, 273-288, 2005.

Thorndycraft, V. R., Bendle, J. M., Benito, G., Davies, B. J., Sancho, C., Palmer, A. P., Fabel, D., Medialdea, A., and Martin, J. R. V.: Glacial lake evolution and Atlantic-Pacific drainage reversals during deglaciation of the Patagonian Ice Sheet, Quat. Sci. Rev., 203, 102-127, https://doi.org/10.1016/j.quascirev.2018.10.036, 2019.

Turner, K. J., Fogwill, C. J., McCulloch, R. D., and Sugden, D. E.: Deglaciation of the eastern flank of the north patagonian icefield and associated continental-scale lake diversions, Geogr. Ann. Ser. A Phys. Geogr., 87, 363-374, 10.1111/j.0435-3676.2005.00263.x, 2005.

Van Daele, M., Bertrand, S., Meyer, I., Moernaut, J., Vandoorne, W., Siani, G., Tanghe, N., Ghazoui, Z., Pino, M., and Urrutia, R.: Late Quaternary evolution of Lago Castor (Chile, 45.6 S): Timing of the deglaciation in northern Patagonia and evolution of the southern westerlies during the last 17 kyr, Quat. Sci. Rev., 133, 130-146, http://dx.doi.org/10.1016/j.quascirev.2015.12.021, 2016.

Villa-Martínez, R., Moreno, P. I., and Valenzuela, M. A.: Deglacial and postglacial vegetation changes on the eastern slopes of the central Patagonian Andes (47°S), Quat. Sci. Rev., 32, 86-99, https://doi.org/10.1016/j.quascirev.2011.11.008, 2012.

Weller, D., De Porras, M., Maldonado, A., Méndez, C., and Stern, C.: Holocene tephrochronology of the lower Río Cisnes valley, southern Chile, Andean Geol., 44, 229-248, 10.5027/andgeoV44n3-a01, 2017.

Weltje, G. J., Bloemsma, M. R., Tjallingii, R., Heslop, D., Rohl, U., and Croudace, I. W.: Prediction of Geochemical Composition from XRF Core Scanner Data: A New Multivariate Approach Including Automatic Selection of Calibration Samples and Quantification of Uncertainties, in: Micro-XRF Studies of Sediment Cores: Applications of a non-destructive tool for the environmental sciences, edited by: Croudace, I. W., and Rothwell, R. G., 17, Springer, 507-534, 2015.